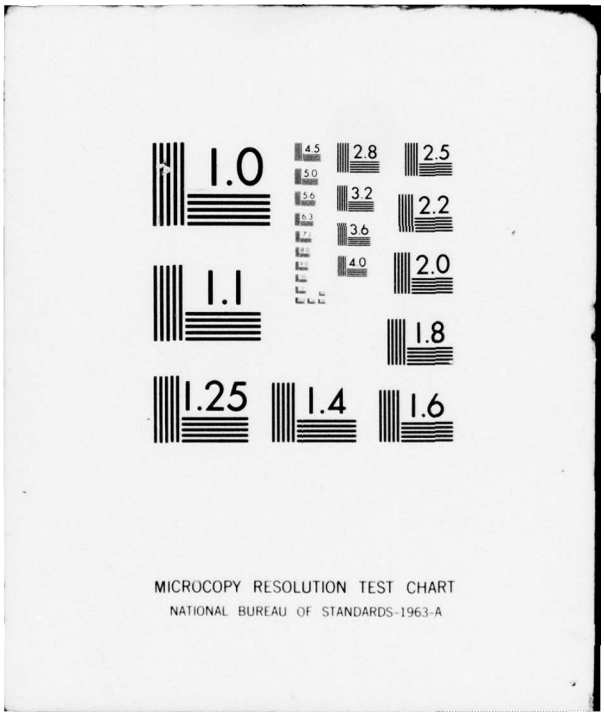
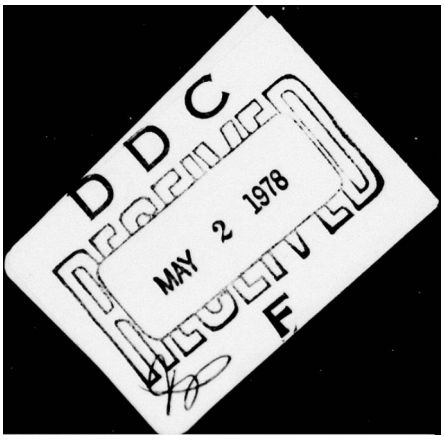
AD-A053 445 AIR FORCE INST OF TECH WRIGHT-PATTERSON AFB OHIO SCH--ETC F/G 5/8
IMPROVING AIDED TRACK PEPFORMANCE DURING PERIODS OF TRACKER SEN--ETC(U)
DEC 77 J G TERRY

UNCLASSIFIED AFIT/GA/EE/77-6 NL



END
DATE FILMED
6 -78
DDC


1.0
1.1
1.25
1.4
1.6
1.8
2.0
2.2
2.5
2.8
3.2
3.6
4.0
4.5
5.0
5.6
6.3
7.1
MICROCOPY RESOLUTION TEST CHART
NATIONAL BUREAU OF STANDARDS-1963-A


DDC
MAY 2 1978
F

AFIT/GA/EE/77-6

AD A053445



DDC
MAY 2 1978
F

AD No.
DDC FILE COPY

IMPROVING AIDED TRACK PERFORMANCE DURING PERIODS OF TRACKER SENSOR FAILURE BY UTILIZING A TARGET BODY FIXED COORDINATE SYSTEM

THESIS

AFIT/GA/EE/77-6

James G. Terry
Captain USAF

Approved for public release; distribution unlimited

AFIT/GA/EE/77-6

IMPROVING AIDED TRACK PERFORMANCE DURING PERIODS OF TRACKER SENSOR FAILURE BY UTILIZING A TARGET BODY FIXED COORDINATE SYSTEM.

Master's THESIS.

Presented to the Faculty of the School of Engineering

of the Air Force Institute of Technology

Air University

in Partial Fulfillment of the

Requirements for the Degree of

Master of Science

by

James G./Terry, B.S.

Captain USAF

Graduate Astronautical Engineering

December 1977

70 p.

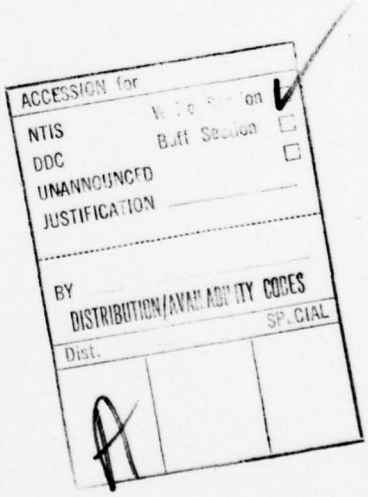
Approved for public release; distribution unlimited

AD A12 225

Preface

During a discussion with my thesis advisor at the beginning of this investigation, I first mentioned the idea of utilizing a rotating, body fixed coordinate system as a possible solution. If I had gotten that idea at any other time, it probably would have died. My advisor caught the significance of that particular solution method, however, and he was able to point me down the investigative path that resulted in this thesis. I don't know of any other advisor who was so willing to spend as much time discussing results, reviewing drafts, or resolving problems with his students as he was. I feel quite fortunate to have had Captain James E. Negro as my thesis advisor. Thanks, Jim.

J. G. T.



Contents

	Page
Preface	ii
List of Figures	v
List of Tables	vi
List of Symbols	vii
Abstract	viii
I. Introduction	1
Background	1
Problem Statement	1
Proposed Solution	2
Investigation Method	3
Thesis Organization	3
II. Scope of Investigation and Assumptions	5
III. Algorithm Modification	7
Original Algorithm	7
Overall System Description	7
Propagation	7
Updating	9
Coast Mode	9
Modified Algorithm	10
Modification Rationale	10
Analytic Development	11
Propagation	13
Updating	19
Coast Mode	20
IV. Investigation	21
Method	21
Target Paths	22
Error Simulation	22
Random Measurement Errors	22
Gyro Drift Errors	24
V. Results and Discussion	25
Results	25
Tables	25
Graphs	25
Discussion	35
Path A Discussion	35
Path B Discussion	40
Path C Discussion	41

Contents

	Page
VI. Conclusions and Recommendations.	43
Conclusions	43
Recommendations	44
Bibliography.	46
Appendix A: Computer Program Modification Listings	47
Appendix B: Simulated Target Paths	56
VITA.	58

List of Figures

Figure		Page
1	Simplified Functional Block Diagram of One Channel of the Control System	8
2	U Coordinate System	12
3	State Vectors Expressed in U Coordinate System	13
4	I, U System Transformation	16
5	Summary of Propagation Equations from Time t to Time t + ΔT	20
6	Illustration of Three Investigated Target Paths	23
7	Azimuth Pointing Error versus Time, Various TVAN Times, Path A	27
8	Elevation Pointing Error versus Time, Various TVAN Times, Path A	28
9	Azimuth Pointing Error versus Time, Various TVAN Times, Path B	30
10	Elevation Pointing Error versus Time, Various TVAN Times, Path B	31
11	Azimuth Pointing Error versus Time, Various TVAN Times, Path C	33
12	Elevation Pointing Error versus Time, Various TVAN Times, Path C	34
13	Actual and Estimated Magnitudes of $\ddot{X}_2(t)$, Path A, TVAN = 3.0 Seconds, for Unmodified and Modified Algorithms, Measurement Uncertainties Included	38
14	Actual and Estimated Magnitudes of $\ddot{X}_2(t)$, Path A, TVAN = 3.0 Seconds, for Unmodified and Modified Algorithms, Measurement Uncertainties Not Included	39

List of Tables

Table		Page
I	Coast Mode RMS Angular Pointing Error Comparison, Path A	26
II	Coast Mode RMS Angular Pointing Error Comparison, Path B	29
III	Coast Mode RMS Angular Pointing Error Comparison, Path C	32

List of Symbols

Symbol	Explaination
$\bar{A}$	Target acceleration vector
A_V, A_L	Components of $\bar{A}$ expressed in the U coordinate system
A_k, k = 1,2,3	Components of $\bar{A}$ expressed in an arbitrary inertial coordinate system
I	Inertial coordinate system defined at start of propagation
$\bar{i},\bar{j},\bar{k}$	Orthogonal set of unit vectors of the I coordinate system
ln	Natural logarithm operator
p_Z	Time derivative operator in the subscripted coordinate frame
$\bar{R}$	Target position vector
R_i, R_j, R_k	Components of $\bar{R}$ expressed in the I coordinate system
R_k, k = 1,2,3	Components of $\bar{R}$ expressed in an arbitrary inertial coordinate system
t	Current time
TVAN	Coast mode initiation time
U	Target body fixed, rotating coordinate system
$\bar{u}_V$, $\bar{u}_L$, $\bar{u}_N$	Orthogonal set of unit vectors of the U coordinate system
$\bar{V}$	Target velocity vector
V	Magnitude of $\bar{V}$
$\bar{V}_A$	Average target vector velocity during propagation period
V_k, k = 1,2,3	Components of $\bar{V}$ expressed in an arbitrary inertial coordinate system
$\bar{W}_{IU}$	Rotation rate of the U system with respect to the I system
W_{IU_V},W_{IU_L},W_{IU_N}	Components of $\bar{W}_{IU}$ expressed in the U coordinate system
X	Cross product operator
X_1,X_2,X_3	Components of computer simulation defined inertial system
$\theta(t)$	Angle through the U system has rotated since t = 0
ΔT	Filter propagation interval (0.1 seconds)
$\overline{\Delta V}$	Change in $\bar{V}$ from t = 0 until t = ΔT
$\dot{Z}$, $\ddot{Z}$	First and second scalar time derivatives of Z

Abstract

A new target acceleration model capable of improving the performance of an airborne aided track system during periods of tracker sensor failure was investigated. An aided track target prediction algorithm utilizing range and angle rate measurements was modified so that the target state estimates were propagated by integrating the estimated constant, body fixed acceleration.

The modified algorithm performance was compared to the original by simulating three target paths. At specified times, all tracking sensors were turned off to simulate sensor failure. Each algorithm attempted to keep the target centered on the tracker boresight by extrapolating target position estimates without processing any measurements. RMS pointing errors were computed for the one second periods following each failure.

During normal sensor operations, the performance of the modified algorithm was equivalent to the original. When the sensors were failed during the tracking of targets following a constant, body fixed acceleration, the modified algorithm generally produced smaller RMS errors. (After 2.8 seconds of filter operating time, the modified algorithm produced one third the RMS error of the original.) When sensor failure occured during the tracking of targets following a rapidly oscillating path or traveling in a straight line under large linear accelerations, both algorithms produced equivalent RMS errors. The modified algorithm demonstrated the same sensitivity to measurement uncertainties as the original.

IMPROVING AIDED TRACK PERFORMANCE DURING PERIODS OF TRACKER SENSOR FAILURE BY UTILIZING A TARGET BODY FIXED COORDINATE SYSTEM

I. Introduction

Background

The accuracy requirements that exist for present day pointing and tracking systems have become so precise that conventional feedback controllers have not been able to solely satisfy them. One system of interest, used to track airborne vehicles, uses Kalman filter estimation techniques to improve the system tracking error characteristics. This system produces real time estimates of the position, velocity, and acceleration of a target. These estimates are then processed and used as additional command signals to the tracker gimbal controls. These signals are called aiding signals, and they are designed to minimize the dynamic lag following errors that occur whenever a target is tracked. (Ref 1:25-38)

Problem Statement

The particular tracking system described in Ref 1 is designed to operate with the sensors periodically providing discrete target information (angle rate and range) to the aided track algorithm. (This condition will be refered to as the normal mode.) However, the target tracking sensors do not always regularly provide information because they cannot always detect the target. Such conditions could be caused by momentary sensor failure, various target orientations, jamming, or atmospheric conditions. During these periods of sensor blackout, current information about the target is no longer available to the tracker gimbal controller. However, the system can utilize the last information that it processed before

sensor blackout and extrapolate estimates of the target position, velocity, and acceleration to future times. (Such a procedure will be refered to as the coast mode.)

During the coast mode, commands can still be provided to the gimbal controls in an attempt to keep the target aligned with the boresight of the inoperative sensors. If an aided track algorithm is designed that provides a better estimate of target motion during the coast mode, then the system will keep the target more accurately aligned with the sensor boresight. When the coast mode ends and the sensors operate again, the better estimate of the true target motion will result in a smaller pointing error and a quicker reacquisition of the target. This thesis develops and investigates the performance of an aided track algorithm modification that improves the performance of this particular tracking system during periods of sensor blackout.

Proposed Solution

The performance of the system to be modified during this investigation relies heavily on the simplified dynamic model used to represent the target in the aided track algorithm. This model represents the target as a point mass possessing inertial position, velocity, and acceleration vectors. These three vectors completely describe the dynamic state of the target. The present algorithm model also assumes that the inertial acceleration of the target remains constant. The future position and velocity are estimated by simply integrating forward that constant acceleration.

Aerodynamic vehicles, however, do not generally possess constant inertial accelerations. Rather, the accelerations experienced by aircraft and airborne missiles are due, for the most part, to specific lift (as a result of the operation of lifting and control surfaces) and specific

lift (through the application of thrust or drag producing devices). These accelerations are closely associated with the target body fixed axes. The algorithm studied in this thesis utilizes the approximation that the non-gravitational target acceleration remains constant with respect to a target body fixed coordinate system.

Investigation Method

The solution to the problem posed by this thesis was investigated by computer simulation. A computer program, described in Ref 2, that modeled the time response of a tracking system was run on the CDC 6600 computer located at Wright-Patterson Air Force Base, Ohio. This program modeled the physical and electronic parameters of the tracking system as well as the time behavior of the target, tracker base, and disturbance inputs. (Ref 3:7) The program was modified during the thesis investigation to incorporate different target trajectories, to modify the aided track algorithm of the present system, to add a coast mode simulation, to simulate range and pointing error uncertainties and gyro drifts, and to add a data output section.

Thesis Organization

This thesis is divided into six chapters and includes two appendices. Chapter II states the assumptions made during the study to simplify calculations and limit the scope of the investigation. Chapter III describes the original algorithm and then mathematically develops the modified algorithm based on the body fixed acceleration assumption. Chapter IV describes how the investigation was conducted and Chapter V presents tabular and graphical results of the investigation. Chapter V also discusses those results in detail. Conclusions and recommendations for future study are listed in Chapter VI. Appendix A provides a detailed account of how the original computer simulation program was modified during the investigation.

Appendix B provides a detailed description of the three different target paths simulated during this thesis study.

II. Scope of Investigation and Assumptions

During the investigation of this thesis, a number of assumptions were made in order to limit the scope of the investigation. The tracker base was assumed to be motionless in all cases, so that, for analysis purposes, the system dynamics would be driven solely by target motion. Also during this study, the effects of acceleration due to gravity were neglected. These first two assumptions were made because during the operation of the actual system, both base motion and gravity can be computed and their effects accounted for.

Coast modes one second in duration were investigated. The target was assumed to be a point target so that tracker pointing errors caused by the system locking-on to different parts of a target would not be considered. Also, only a complete, simultaneous loss of range, angle rate, and pointing error sensors was considered. Intermittent or partial sensor failure was not investigated. It was also assumed that any sensor failures would be detected by the system, so that erroneous measurements due to any failures would not be included in the target state estimation calculations.

A real target can change acceleration, within certain physical limits, in an unpredictable fashion. If this occurs, the target trajectory will also be changed unpredictably. After a sensor blackout, any unmodeled acceleration changes to a trajectory even perfectly known prior to blackout will cause pointing errors. Rather than model the possible effects of these uncertainties, it was assumed that any state estimation errors caused by acceleration changes after a sensor blackout would equally affect the pointing error performance of the present and proposed algorithms. Therefore, the target trajectories that were produced by the computer simulation during this investigation were deterministically rather than randomly generated.

Finally, the sole performance criterion for comparing algorithms in this study was root mean squared (RMS) tracker pointing error. If the RMS pointing error produced by one algorithm during a one second coast mode period was smaller than that produced by the other algorithm for the identical period, then the first algorithm was assumed to be better. The instantaneous error present at the end of a coast mode period is more important than RMS error because of the major effect such an error would have on the reacquisition dynamics of the system. However, the reacquisition time of the system will not occur at a precisely known time, so the RMS error computed over the whole coast mode period will give a better, overall measure of the performance for a range of possible reacquisition times.

III. Algorithm Modification

Original Algorithm

Overall System Description. To place the following discussion of the aided track algorithm into context, a short description of the overall tracking system is provided in this subsection.

The angular rate command signal (azimuth or elevation) that is provided to the respective gimbal actuator is the sum of two separate signals. One of these signals, called the tracker controller signal, is produced by a proportional plus integral feedback scheme that uses the angular error detected by a tracker/imager as the feedback error signal. (Ref 2:3-5) The tracker controller provides the only tracking commands until the aided track algorithm is activated.

The other part of the angular rate command, called the aiding signal, is produced by the aided track algorithm as it processes range and angular rate measurements. The aided track algorithm is described in greater detail in the remainder of this section. A simple functional block diagram describing the control system is provided in Fig 1.

Propagation. The original aided track algorithm propagates the estimates of the target state vectors from one update time to the next. The dynamic model that this algorithm employs was based on the assumption that the target is a point mass that has associated with it three estimated state vectors; inertial acceleration, inertial velocity, and inertial position. The estimated inertial acceleration is assumed to be constant and the velocity and position estimates are propagated by simply integrating forward that constant acceleration. Mathematically this can be

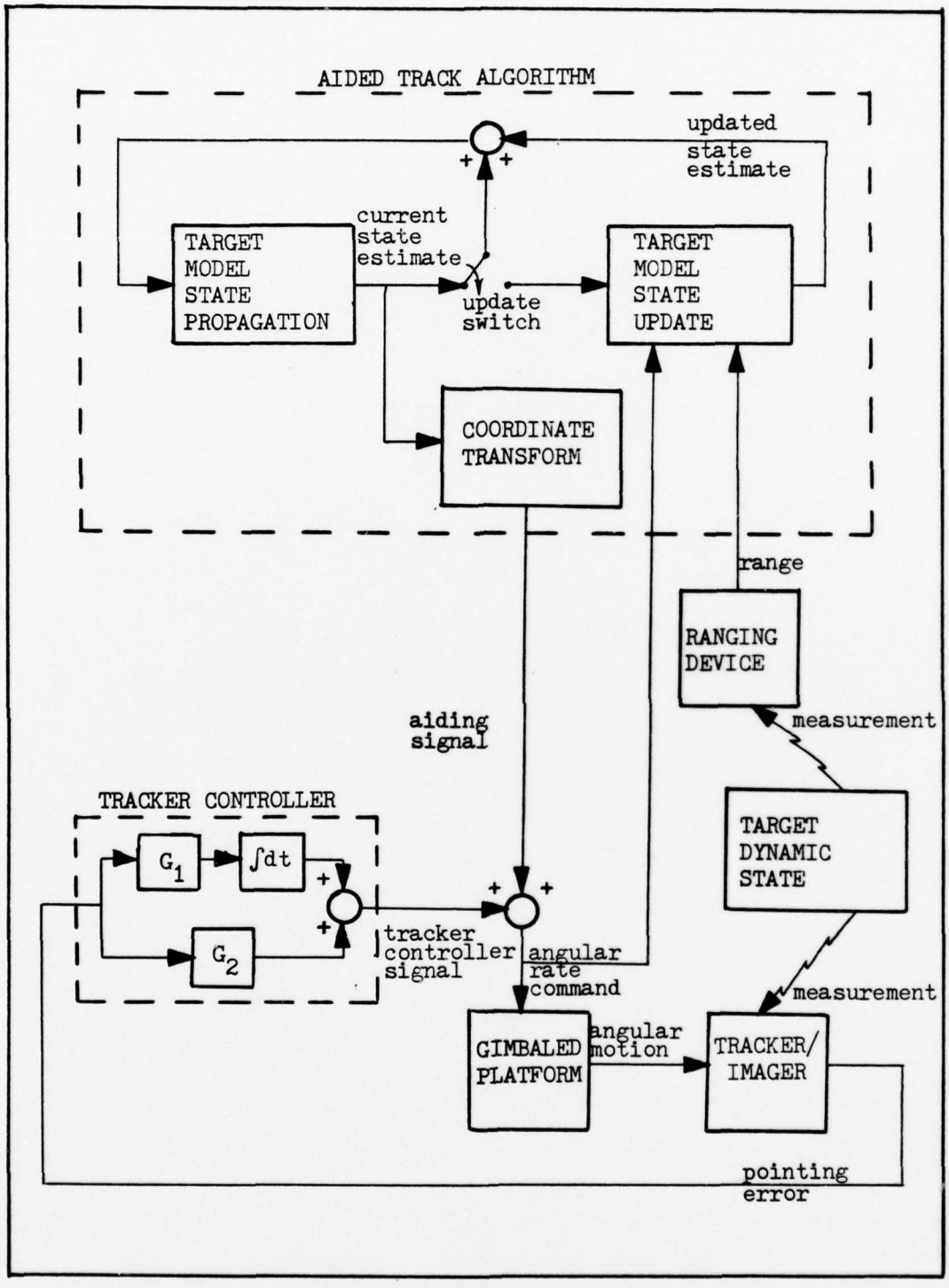


Figure 1. Simplified Functional Block Diagram
of One Channel of the Control System

expressed as

$$\begin{bmatrix} R_k(t+\Delta T) \\ V_k(t+\Delta T) \\ A_k(t+\Delta T) \end{bmatrix} = \begin{bmatrix} 1 & \Delta T & \frac{\Delta T^2}{2} \\ 0 & 1 & \Delta T \\ 0 & 0 & 1 \end{bmatrix} \begin{bmatrix} R_k(t) \\ V_k(t) \\ A_k(t) \end{bmatrix} \quad (1)$$

where k = 1, 2, 3 (the three axes of an inertial Catresian coordinate system), t is the current time, ΔT is the time increment over which the target states are being propagated, and R_k, V_k, and A_k are the k^{th} components of the inertial position, velocity, and acceleration vectors, respectively. (Ref 1:32)

The current estimates of position, velocity, and acceleration are converted through a coordinate transformation into estimates of the required gimbal azimuth and elevation rates. The aided track algorithm then produces aiding signals that are added to the tracker controller commanded signals. (Ref 1:5)

Updating. At each update time, angle rate and range measurements are taken. These measurements are transformed into a rectangular set of (so called) pseudo measurements which consist of three components of position and three components of velocity. (Ref 1:30-31) The Kalman filter combines the pseudo measurements with the current estimates and produces an updated set of estimated target state vectors. (Ref 1:33) These updated estimates are then propagated by the aided track algorithm to the next update time. The fundamental matrix of this algorithm models the acceleration of the target as a random walk phenomenon. (Ref 1:34)

Coast Mode. The original computer simulation did not provide for a coast mode of operation. As originally programmed, when the simulated target could no longer be detected by the tracker sensors, the entire simulation was terminated. (Ref 2:35-36) The program was modified, therefore, so that this important phase of operation could be investigated.

This subsection describes the performance of the original system after it was modified to allow the simulation of the coast mode.

Just as in the normal mode, the estimated state vectors are propagated to the next update time. However, no measurements can be taken at that time because of the sensor blackout, and the Kalman gain equations are not processed to avoid calculations with erroneous data. Instead, updating does not take place and the state estimates simply remain unchanged. This process of propagating without updating is continued until the coast mode ends and normal sensor measurements are again available.

During a sensor blackout the pointing error signals obtained from the tracker/imager are unreliable. At the beginning of the coast mode, therefore, the pointing error signals are set to zero. This rate memory mode of operation holds the tracker controller signal constant at a value equal to the last integrator output value. The aided track algorithm continues to provide an aiding signal based on the current, nonupdated estimates of the target state vectors.

Modified Algorithm

Modification Rationale. The original algorithm assumed that the acceleration of an aerodynamic vehicle (caused by the forces of thrust, list, and drag) is inertially constant. (This analysis neglects gravity.) However, in the aerodynamic vehicles that will be tracked by this system thrust is produced by engines fixed in the vehicles. In addition, lift and drag are defined as the perpendicular forces resulting from aerodynamic effects on the vehicles. The directions of these aerodynamic forces are defined with respect to the velocities of the vehicles, not inertial space. As the vehicles maneuver, the orientations of thrust and these aerodynamic forces also change with respect to inertial space.

These forces are not necessarily constant with respect to a target fixed coordinate system, but they are more closely associated with such a system than with an inertially fixed system, especially if the target is maneuvering. Such an observation about the forces that act on aircraft and airborne missiles suggests that, to improve tracker performance, the original algorithm could be modified. The resulting modification is based on the assumption that, neglecting the acceleration caused by gravity, the magnitude and direction of the acceleration of an airborne vehicle are constant with respect to the vehicle itself.

Because a pilot (or missile controller) can change the throttle setting or angle of attack of a target vehicle at any time, the target body fixed acceleration will generally not be constant. However, if such changes are assumed to be pertubations in a constant, target body fixed acceleration, then an estimate of that acceleration can be produced and propagated by the Kalman filter. The resulting target state estimates can be transformed into aiding signals and added to the tracker controller signals as in the original system.

Because this model represents an actual aircraft more realistically than the original model, it is reasonable to expect better performance during the coast mode from the modified algorithm if an aircraft is tracked. The remainder of this thesis develops and investigates this proposed modification.

Analytic Development. To take advantage of the knowledge of the dynamics of the target vehicles, a target model with a constant, body fixed acceleration was developed to be used in the propagation portion of the aided track algorithm. As the new target model rotates, the estimated acceleration vector is also rotated about the same axis, and the magnitude

of the acceleration remains constant. (This model happens to represent perfectly an aircraft performing a level, constant rate, constant airspeed turn.)

Information about the target orientation is not available to the algorithm from the tracker sensors. Therefore, the longitudinal axis of the target model was defined in the modified algorithm to coincide with the estimated velocity vector. A second coordinate direction was defined to coincide with the vector cross product of the estimated velocity and estimated acceleration vectors. The third body fixed coordinate was defined to complete a right handed, orthogonal set.

These directions make up the U coordinate system which is defined at any time t by the following unit vectors.

$$\bar{u}_V(t) = \frac{\bar{V}(t)}{|\bar{V}(t)|} \tag{2}$$

$$\bar{u}_N(t) = \frac{\bar{V}(t) \times \bar{A}(t)}{|\bar{V}(t) \times \bar{A}(t)|} \tag{3}$$

$$\bar{u}_L(t) = \bar{u}_N(t) \times \bar{u}_V(t) \tag{4}$$

where the superior bar represents vector quantities, $\bar{V}(t)$ is the estimated inertial velocity, $\bar{A}(t)$ is the estimated inertial acceleration, X is the cross product operator, $\bar{u}_V(t)$ is a unit vector in the direction of $\bar{V}(t)$, $\bar{u}_N(t)$ is a unit vector in the direction of $\bar{V}(t) \times \bar{A}(t)$, and $\bar{u}_L(t)$ is a unit vector that completes the set. Fig 2 illustrates the U system.

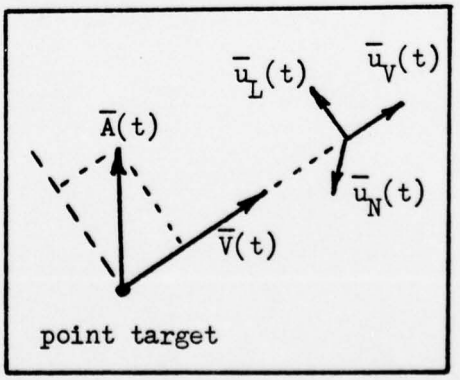


Figure 2. U Coordinate System

Propagation. The purpose of the propagation section of this algorithm is to find the estimated future values of $\bar{A}(t + \Delta T)$, $\bar{V}(t + \Delta T)$, and $\bar{R}(t + \Delta T)$ given the current best estimates of $\bar{A}(t)$, $\bar{V}(t)$, and $\bar{R}(t)$. The following subsection of this thesis develops the equations to find those estimated future values.

The estimated inertial acceleration and velocity vectors of the target can be defined at any time t in terms of the rotating U coordinate system and scalar quantities as

$$\bar{A}(t) = A_V(t)\bar{u}_V(t) + A_L(t)\bar{u}_L(t) \tag{5}$$

$$\bar{V}(t) = V(t)\bar{u}_V(t) \tag{6}$$

These vectors, along with $\bar{R}(t)$, the estimated position vector, are illustrated in Fig 3.

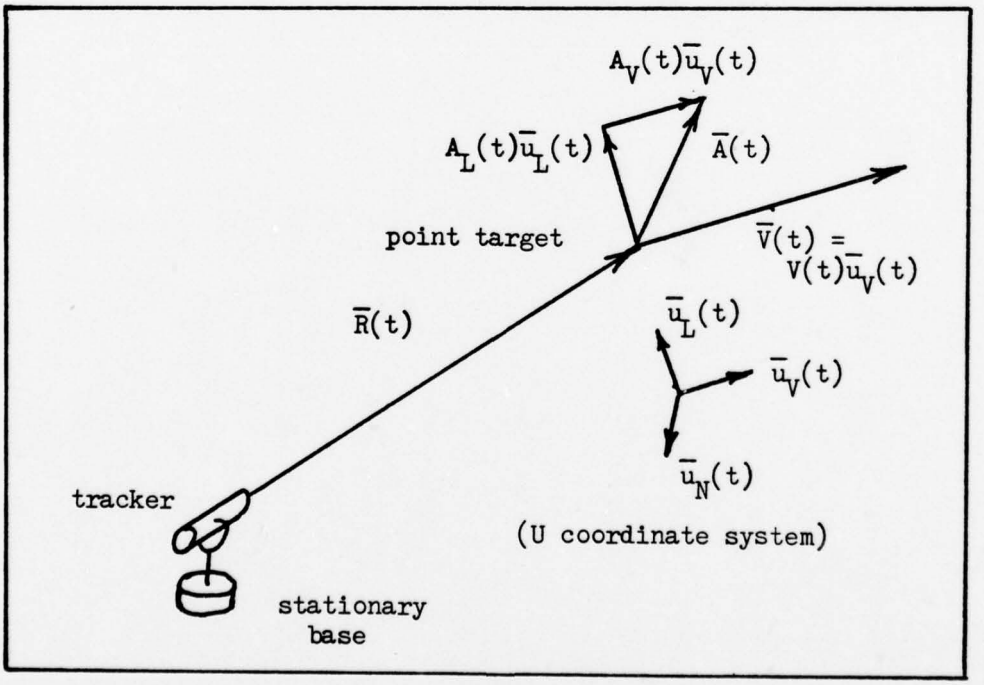


Figure 3. State Vectors Expressed in U Coordinate System

The modified algorithm propagates the state estimates by assuming that the components of acceleration remain constant during the short time period, ΔT, so that $A_V(t) = A_V(t + \Delta T)$ and $A_L(t) = A_L(t + \Delta T)$. The estimated acceleration and velocity vectors for time $t + \Delta T$ are then found to be

$$\bar{A}(t + \Delta T) = A_V(t)\bar{u}_V(t + \Delta T) + A_L(t)\bar{u}_L(t + \Delta T) \tag{7}$$

$$\bar{V}(t + \Delta T) = V(t + \Delta T)\bar{u}_V(t + \Delta T) \tag{8}$$

The scalar $V(t + \Delta T)$ can be found by vector calculus as follows.

The acceleration vector can be represented by applying the Theorem of Coriolis to $\bar{V}(t)$.

$$p_I\bar{V}(t) = p_U\bar{V}(t) + \bar{W}_{IU}(t) \times \bar{V}(t) \tag{9}$$

where I represents an inertial coordinate system, p represents the time derivative operator in the subscripted coordinate system, and $\bar{W}_{IU}(t)$ is the angular rate of the U system with respect to the I system. Expressed in the U coordinate system, $\bar{W}_{IU}(t)$ is

$$\bar{W}_{IU}(t) = W_{IU_V}(t)\bar{u}_V(t) + W_{IU_L}(t)\bar{u}_L(t) + W_{IU_N}(t)\bar{u}_N(t) \tag{10}$$

If equation (9) is coordinatized in the U system, the following is obtained:

$$\begin{bmatrix} A_V(t) \\ A_L(t) \\ 0 \end{bmatrix}^U = \begin{bmatrix} \dot{V}(t) \\ 0 \\ 0 \end{bmatrix}^U + \begin{bmatrix} 0 & -W_{IU_N}(t) & W_{IU_L}(t) \\ W_{IU_N}(t) & 0 & -W_{IU_V}(t) \\ -W_{IU_L}(t) & W_{IU_V}(t) & 0 \end{bmatrix}^U \begin{bmatrix} V(t) \\ 0 \\ 0 \end{bmatrix}^U \tag{11}$$

where the superscripts represent the reference system of coordinatization, the superior dot represents the scalar time derivative, and the 3 by 3 matrix is the skew symmetric form of $\bar{W}_{IU}(t)$. (Ref 4:22)

From matrix equation (11), the following scalar equations can be obtained:

$$\dot{V}(t) = A_V(t) \tag{12}$$

$$W_{IU_N}(t) = \frac{A_L(t)}{V(t)} \tag{13}$$

$$W_{IU_L}(t)V(t) = 0 \tag{14}$$

Since $W_{IU_V}(t)$ does not appear in these scalar equations, it cannot be found mathematically from them. This component of $\bar{W}_{IU}(t)$ represents target roll. There are many possible methods to model target roll, but in this development target roll will be assumed to be zero so that $W_{IU_V}(t) = 0$. Also, because in general $V(t) \neq 0$, equation (14) results in $W_{IU_L}(t) = 0$. Therefore

$$\bar{W}_{IU}(t) = W_{IU_N}(t)\bar{u}_N(t) \tag{15}$$

Because $A_V(t)$ has been assumed to be constant, simple scalar integration of equation (12) from time = t to time $t = t + \Delta T$ yields

$$V(t + \Delta T) = A_V(t)\Delta T + V(t) \tag{16}$$

At this point in the derivation of the new propagation equations, it is convenient to redefine time as $t = 0$ at the beginning of each propagation cycle. Without loss of generality, the inertial coordinate system I, composed of unit vectors $\bar{i}$, $\bar{j}$, and $\bar{k}$, can also be defined at the beginning of each propagation cycle so that the U system and the I system coincide at $t = 0$. ($\bar{u}_V(0) = \bar{i}$, $\bar{u}_L(0) = \bar{j}$, and $\bar{u}_N(0) = \bar{k}$) The unit vectors of the rotating U system can be found at any time in terms of the non-rotating I system as

$$\bar{u}_V(t) = \cos[\theta(t)]\bar{i} + \sin[\theta(t)]\bar{j} \tag{17a}$$

$$\bar{u}_L(t) = -\sin[\theta(t)]\bar{i} + \cos[\theta(t)]\bar{j} \tag{17b}$$

$$\bar{u}_N(t) = \bar{k} \tag{17c}$$

where $\theta(t)$ is the angle through which the U system has rotated since $t = 0$.

This relationship is only valid for $0 \leq t \leq \Delta T$. When $t = \Delta T$, time is redefined as $t = 0$ and a new I coordinate system is defined for the next propagation cycle. The relationship between the U and I coordinate systems is illustrated in Fig 4.

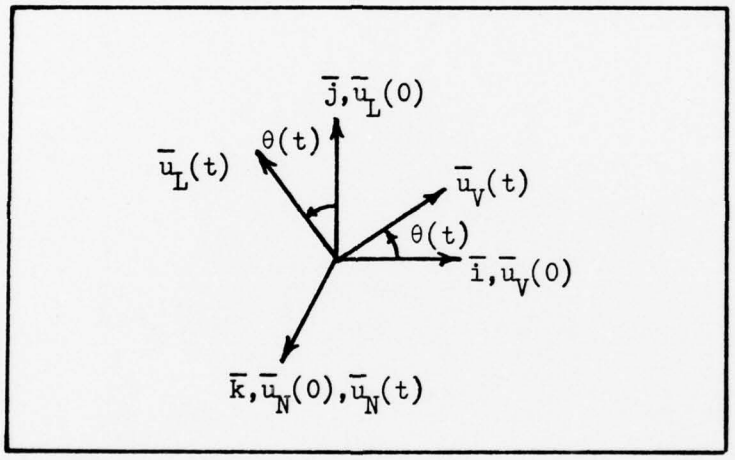


Figure 4. I, U System Transformation

The change in the inertial velocity vector that occurs from time $t = 0$ to time $t = \Delta T$ is defined as the vector difference

$$\overline{\Delta V} = \bar{V}(\Delta T) - \bar{V}(0) \tag{18}$$

Substitution of the values for $V(0)$ and $V(\Delta T)$ from equations (6) and (8) into equation (18) yields

$$\overline{\Delta V} = V(\Delta T)\bar{u}_V(\Delta T) - V(0)\bar{u}_V(0) \tag{19}$$

Completing the transformation defined by equation (17) and substituting for $V(\Delta T)$ from equation (16) gives $\overline{\Delta V}$ in terms of inertial coordinates.

$$\overline{\Delta V} = [A_V(0)\Delta T + V(0)]\{\cos[\theta(t)]\bar{i} + \sin[\theta(t)]\bar{j}\} - V(0)\bar{i} \tag{20}$$

Substituting into equation (19) and solving for $V(\Delta T)\bar{u}_V(\Delta T) = \bar{V}(\Delta T)$ yields

$$\bar{V}(\Delta T) = [A_V(0)\Delta T + V(0)]\cos[\theta(t)]\bar{i} + [A_V(0)\Delta T + V(0)]\sin[\theta(t)]\bar{j} \tag{21}$$

$\theta(\Delta T)$ can be found by integrating equation (13).

$$\theta(\Delta T) = \int_0^{\Delta T} W_{IU_N}(t)\, dt = \int_0^{\Delta T} \frac{A_L(t)}{V(t)}\, dt \tag{22}$$

$V(t)$ is given by equation (16) and $A_V(t)$ and $A_L(t)$ are constants. Therefore

$$\theta(\Delta T) = A_L(0) \int_0^{\Delta T} \frac{dt}{A_V(0)t + V(0)} \tag{23}$$

Performing the indicated integration yields

$$\theta(\Delta T) = \frac{A_L(0)}{A_V(0)} \ln\left[\frac{A_V(0)}{V(0)}\Delta T + 1\right], \quad A_V(0) \neq 0 \tag{24}$$

where ln represents the natural logarithm operation.

If the estimated value of $A_V(0) = 0$, the value for $\theta(\Delta T)$ becomes undefined if equation (24) is used. However, if $A_V(0) = 0$, then $V(t) = V(0)$ and the estimated magnitude of $W_{IU_N}(t)$ will be constant during time ΔT. Subsequent integration of equation (23) yields

$$\theta(\Delta T) = \frac{A_L(0)}{V(0)}\Delta T, \quad A_V(0) = 0 \tag{25}$$

which is to be used in place of equation (24) in those cases. $\bar{V}(\Delta T)$ can

be found by substituting the resulting value for $\theta(\Delta T)$ into equation (21).

$\bar{A}(\Delta T)$, the inertial acceleration vector, can be found more directly, because the components $A_V(t)$ and $A_L(t)$ are assumed to be constant. Thus, only a coordinate transformation is required. Applying the coordinate transformation defined in equation (17) to equation (5) and gathering terms result in

$$\begin{aligned}\bar{A}(\Delta T) = {} & \{A_V(0)\cos[\theta(\Delta T)] - A_L(0)\sin[\theta(\Delta T)]\}\bar{i} \\ & + \{A_V(0)\sin[\theta(\Delta T)] + A_L(0)\cos[\theta(\Delta T)]\}\bar{j}\end{aligned} \tag{26}$$

$\bar{R}(\Delta T)$ can be found by integrating the components of $\bar{V}(t)$ from time $t = 0$ to time $t = \Delta T$ and adding the results to $\bar{R}(0)$. However, the resulting integrands contain terms of the form

$$I_1 = \int_0^{\Delta T} \sin\{\frac{A_L(0)}{A_V(0)} \ln[\frac{A_V(0)}{V(0)}t + 1]\}\, dt \tag{27}$$

$$I_2 = \int_0^{\Delta T} \cos\{\frac{A_L(0)}{A_V(0)} \ln[\frac{A_V(0)}{V(0)}t + 1]\}\, dt \tag{28}$$

which have not been solved in closed form.

$\bar{R}(\Delta T)$ is found instead by making the simplifying assumption that during the short time ΔT

$$\bar{R}(\Delta T) = \bar{R}(0) + \bar{V}_A \Delta T \tag{29}$$

where $\bar{V}_A$ is a constant velocity vector that is assumed to have operated during ΔT.

Because $\bar{V}(0)$ and $\bar{V}(\Delta T)$ are both known, the assumption is made that

$$\bar{V}_A = \frac{\bar{V}(0) + \bar{V}(\Delta T)}{2} = \bar{V}(0) + \frac{\overline{\Delta V}}{2} \tag{30}$$

where $\overline{\Delta V}$ is given by equation (20).

Substituting $\bar{V}_A$ into equation (29) results in

$$R(\Delta T) = R(0) + \left[V(0) + \frac{\Delta V}{2}\right]\Delta T \tag{31}$$

$\bar{R}(0)$ is known in terms of the I system as

$$\bar{R}(0) = R_i(0)\bar{i} + R_j(0)\bar{j} + R_k(0)\bar{k} \tag{32}$$

Substituting into equation (31) for $\bar{R}(0)$ from equation (32) and for $\overline{\Delta V}$ from equation (20), then gathering terms gives the desired result:

$$\begin{aligned}\bar{R}(\Delta T) = &\left[R_i(0) + \left\{\frac{V(0)}{2} + \left[A_V(0)\Delta T + V(0)\right]\frac{\cos[\theta(\Delta T)]}{2}\right\}\Delta T\right]\bar{i} \\ &+ \left[R_j(0) + \left\{\left[A_V(0)\Delta T + V(0)\right]\frac{\sin[\theta(\Delta T)]}{2}\right\}\Delta T\right]\bar{j} \\ &+ \left[R_k(0)\right]\bar{k}\end{aligned} \tag{33}$$

If during any propagation cycle the estimated value of either $A_L(0)$ or $V(0)$ is zero, then the definition of the U coordinate system, equations (2), (3), and (4), cannot be applied. In those cases, the modified algorithm is switched back to the original algorithm method of propagation. (In the first case, no target rotation is estimated, and in the second case, the target is estimated to be motionless. In either case, the original algorithm is expected to provide satisfactory propagation.)

A summary of the modified algorithm propagation equations studied in this thesis is listed in Fig 5.

Updating. The equations used in the propagation portion of the modified algorithm cannot be directly incorporated into the Kalman gain equations used in the update portion of the algorithm because they are non-linear. No attempt was made to linearize these equations, rather the original Kalman gain equations from the unmodified algorithm were retained in their original form so that their practical real-time calculation properties could be utilized.

Coast Mode. The coast mode of operation, as described for the original algorithm, was also unchanged in the modified algorithm. The same procedure of propagating without updating was followed to avoid erroneous measurements.

$$\bar{A}(t + \Delta T) = \{A_V(t)\cos[\theta(t + \Delta T)] - A_L(t)\sin[\theta(t + \Delta T)]\}\bar{i} + \{A_V(t)\sin[\theta(t + \Delta T)] + A_L(t)\cos[\theta(t + \Delta T)]\}\bar{j} \quad (26)$$

$$\bar{V}(t + \Delta T) = [A_V(t)\Delta T + V(t)]\cos[\theta(t + \Delta T)]\bar{i} + [A_V(t)\Delta T + V(t)]\cos[\theta(t + \Delta T)]\bar{j} \quad (21)$$

$$\bar{R}(t + \Delta T) = \left[R_i(t) + \{\frac{V(t)}{2} + [A_V(t)\Delta T + V(t)]\frac{\cos[\theta(t + \Delta T)]}{2}\}\Delta T\right]\bar{i} + \left[R_j(t) + \{[A_V(t)\Delta T + V(t)]\frac{\sin[\theta(t + \Delta T)]}{2}\}\Delta T\right]\bar{j} + [R_k(t)]\bar{k} \quad (33)$$

where

$$\theta(t + \Delta T) = \frac{A_L(t)}{A_V(t)}\ln[\frac{A_V(t)}{V(t)}\Delta T + 1] \text{ , } A_V(t) \neq 0 \quad (24)$$

or

$$\theta(t + \Delta T) = \frac{A_L(t)}{V(t)}\Delta T \text{ , } A_V(t) = 0 \quad (25)$$

(ΔT, the estimated values of $A_V(t)$, $A_L(t)$, $V(t)$, $R_i(t)$, $R_j(t)$, $R_k(t)$, and directions of $\bar{i}$, $\bar{j}$, and $\bar{k}$ are known at the beginning of each propagation cycle.)

Figure 5. Summary of Propagation Equations from Time t to Time t + ΔT

IV. Investigation

The problem posed by this thesis was investigated by computer simulation. The CDC 6600 computer located at Wright-Patterson Air Force Base, Ohio, was used to execute the simulation program (described in Ref 2) which modeled the time response characteristics of the tracking system. This program was changed to incorporate the aided track algorithm modifications that were developed in Chapter III of this thesis. A coast mode simulation was also added to the program so that both the normal and coast modes of operation could be studied. Appendix A provides computer listings of the modifications to the original computer simulation program.

Method

This problem was investigated by simulating the tracking of three different, representative target paths and comparing the performance of the original system with that of the modified system. The coast mode initiation time (designated TVAN) was varied during each computer run, so that any system performance sensitivity to shorter or longer filter operating times could be found. The duration of the coast mode was 1.0 seconds for all simulations. The effects of measurement errors were investigated by simulating range and pointing error uncertainties and gyro drifts. During every run the aided track algorithm was turned on at t = 0.2 seconds. The tracker controller alone controlled the system prior to that time.

RMS azimuth and elevation pointing errors were computed during each one second coast mode period. These RMS error values were used as the sole performance criterion during this study.

Two computer runs were made for each set of conditions. One run simulated the modified system; the other simulated the unmodified system.

The two runs were identical except for the insertion of the algorithm modification into the second run. Any difference in performance between the two simulated runs was assumed to be caused by the algorithm modification.

Target Paths

The target paths were designated Path A, Path B, and Path C. Path A simulated a constant speed, circular target motion; Path B simulated a constant speed, sinusoidal target motion; and Path C simulated a straight line target motion under the influence of a high g, one dimensional, inertial acceleration followed by a similar deceleration. These paths are illustrated in Fig 6 and are described in detail in Appendix B.

Error Simulation

The system being studied obtains measurements from three sources. The angular rates that are used as commands to the gimbal actuators are used as the system inertial boresight angular rate measurements, range information is obtained from a ranging device, and tracker boresight error is obtained from an infra-red tracker/imager device. (Ref 2:3) These real devices are affected by errors that the original simulation program did not model. In order to investigate the sensitivity of the modified system to measurement errors or gyro drifts, the computer program was modified to model those effects.

Random Measurement Errors. The original computer program provided a random number generator that was utilized to model the random measurement errors that occur in the real ranging and tracker/imager devices. Three independent sequences of white, Gaussian random numbers with zero means and specified standard deviations were generated and added to the modeled measurements of elevation and azimuth pointing and range errors, respectively. The standard deviations were set at 5.0 meters for the range error and

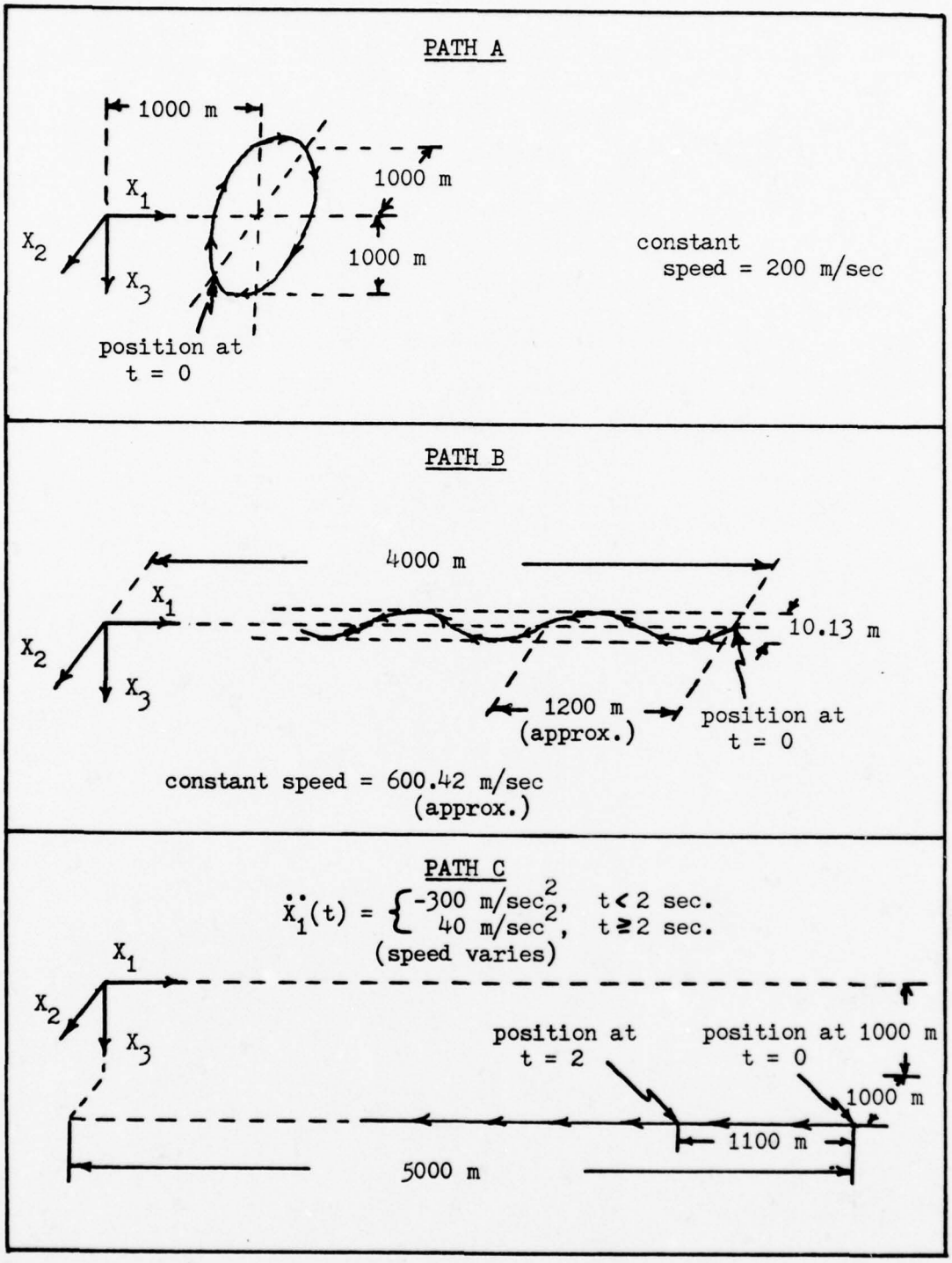


Figure 6. Illustration of Three Investigated Target Paths

10.0 microradians for the two angular measurement errors. It was assumed that all other range or boresight error measurement uncertainties were small when compared to these random measurement errors.

To provide a common basis for comparing results, the same set of random sequences was used for every simulation run. To insure that the choice of one particular set of random sequences did not influence the final results, several simulations runs were made with no uncertainty inputs. By comparing the results of simulations with uncertainty inputs to those without, it could be determined whether this specific set of uncertaintly sequences or the basic difference between the two algorithms caused the results reported later in this study.

Gyro Drift Errors. It was assumed that the only significant contribution to the angular rate measurement errors would be caused by gyro bias drifts. To simulate these errors, a constant value of 0.1 degrees/hour (approximately 0.48 microradians/second) was added to the modeled elevation and azimuth inertial rate values produced by the section of the computer program that simulated the gyro dynamics of the system.

V. Results and Discussion

Results

In this section of the report the results of this investigation are presented in tabular and graphical form. In each of the following tables and graphs, TVAN, the coast mode initiation time, is the varying parameter. Separate tables and graphs are presented for each of the three representative target paths. Those tables and graphs are grouped according to target path.

Tables. Three tables of results are presented. Each table compares the RMS azimuth and elevation pointing errors of the unmodified system with the corresponding errors of the modified system during six different one second coast mode periods. Each coast mode period was initiated at a different TVAN, starting at t = 0.5 seconds and increasing by 0.5 second increments until t = 3.0 seconds. The RMS errors were computed by the computer program for the period t = TVAN until t = TVAN + 1.0 second for each run.

Graphs. Six graphs of results are presented. Alternating graphs plot azimuth or elevation pointing error versus time for both the modified and unmodified systems, one for each target path. The results of varying TVAN for each target path are shown by plotting all the runs for the various TVAN times on the same graph. Each plot ends 1.0 second after the respective TVAN time. Four additional graphs are presented in the Discussion section of this chapter which illustrate the effects of the measurement uncertainties on the system performance and which illustrate the basic difference between the two propagation methods.

Table I

Coast Mode RMS Angular Pointing Error Comparison, Path A

TVAN (Seconds)	Channel	Unmodified Algorithm RMS Error (Milliradians)	Modified Algorithm RMS Error (Milliradians)
0.5	Azimuth	4.4092	4.4094
	Elevation	1.1522	1.1555
1.0	Azimuth	3.9983	4.0010
	Elevation	0.1036	0.1459
1.5	Azimuth	1.3632	1.3590
	Elevation	0.3165	0.1788
2.0	Azimuth	0.4103	0.2847
	Elevation	0.1588	0.0635
2.5	Azimuth	0.9088	0.4113
	Elevation	0.8758	0.3045
3.0	Azimuth	1.0272	0.3492
	Elevation	1.6985	0.6857

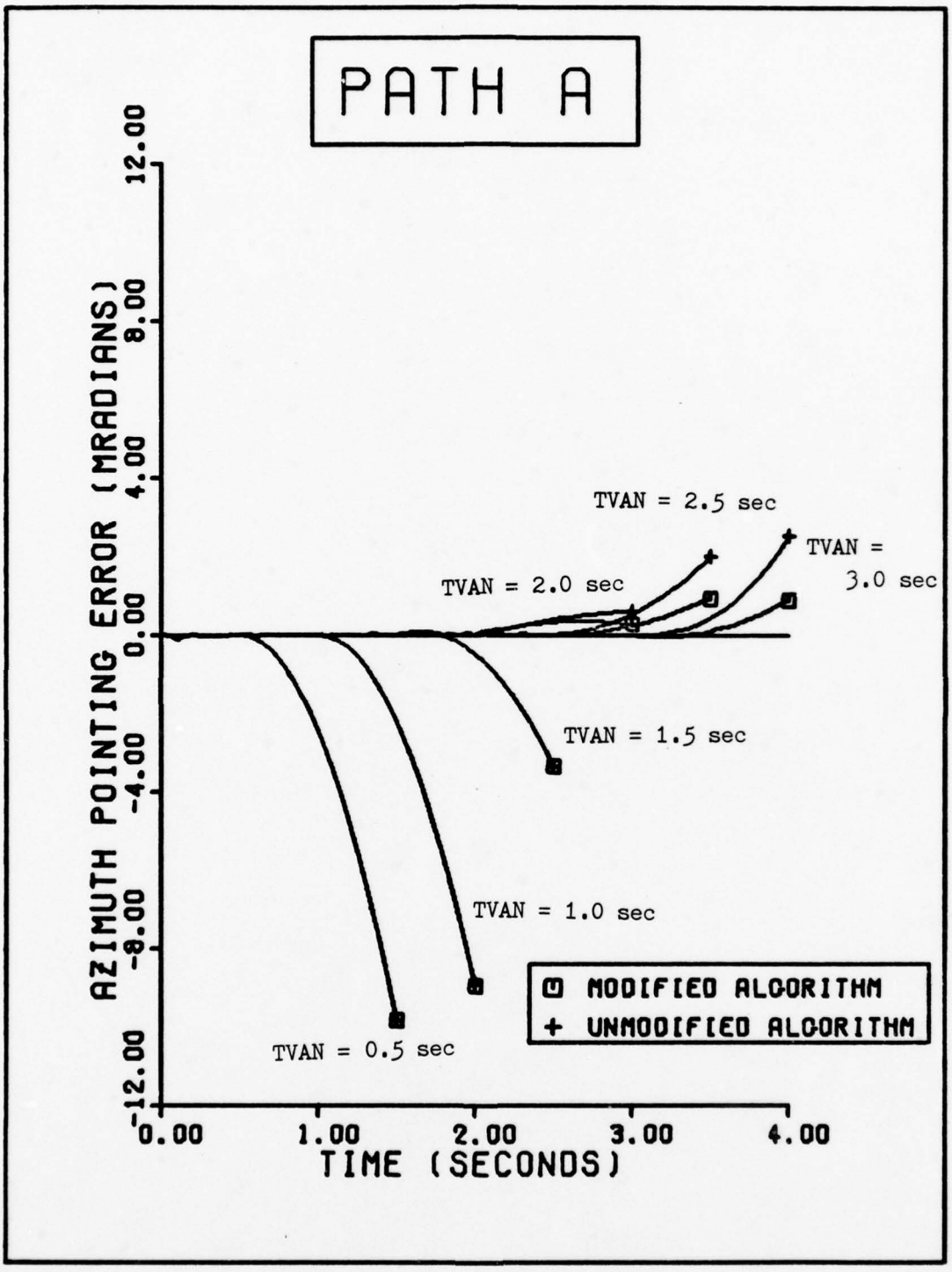


Figure 7. Azimuth Pointing Error versus Time, Various TVAN Times, Path A

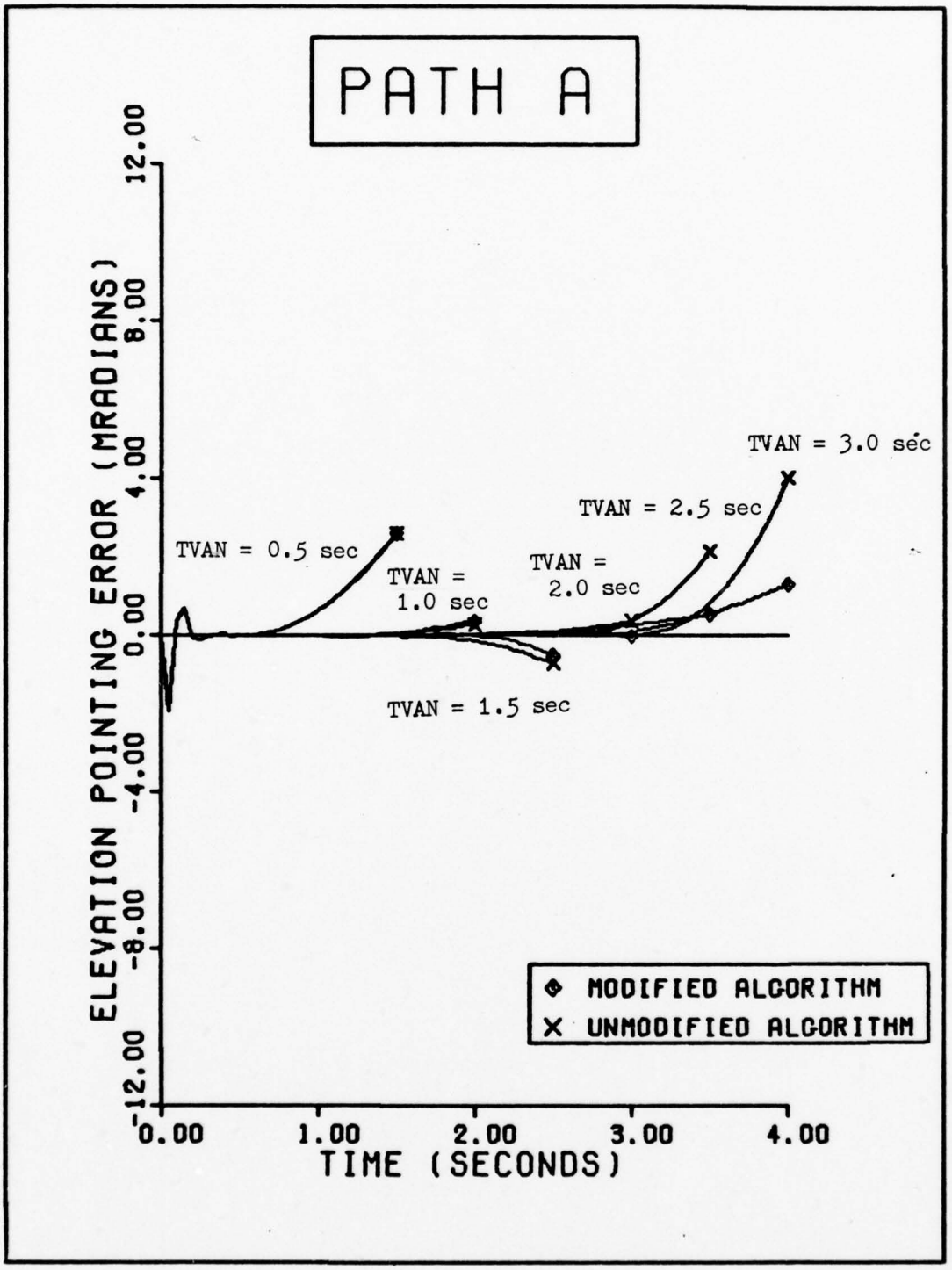


Figure 8. Elevation Pointing Error versus Time, Various TVAN Times, Path A

Table II

Coast Mode RMS Angular Pointing Error Comparison, Path B

TVAN (Seconds)	Channel	Unmodified Algorithm RMS Error (Milliradians)	Modified Algorithm RMS Error (Milliradians)
0.5	Azimuth	3.8033	3.8033
	Elevation	0.1516	0.1527
1.0	Azimuth	5.3652	5.3647
	Elevation	0.0579	0.1265
1.5	Azimuth	6.4504	6.4449
	Elevation	0.0184	0.0419
2.0	Azimuth	10.2466	10.2210
	Elevation	0.0457	0.4373
2.5	Azimuth	11.6687	11.6216
	Elevation	0.1487	0.0419
3.0	Azimuth	11.5772	11.6858
	Elevation	0.0451	0.1642

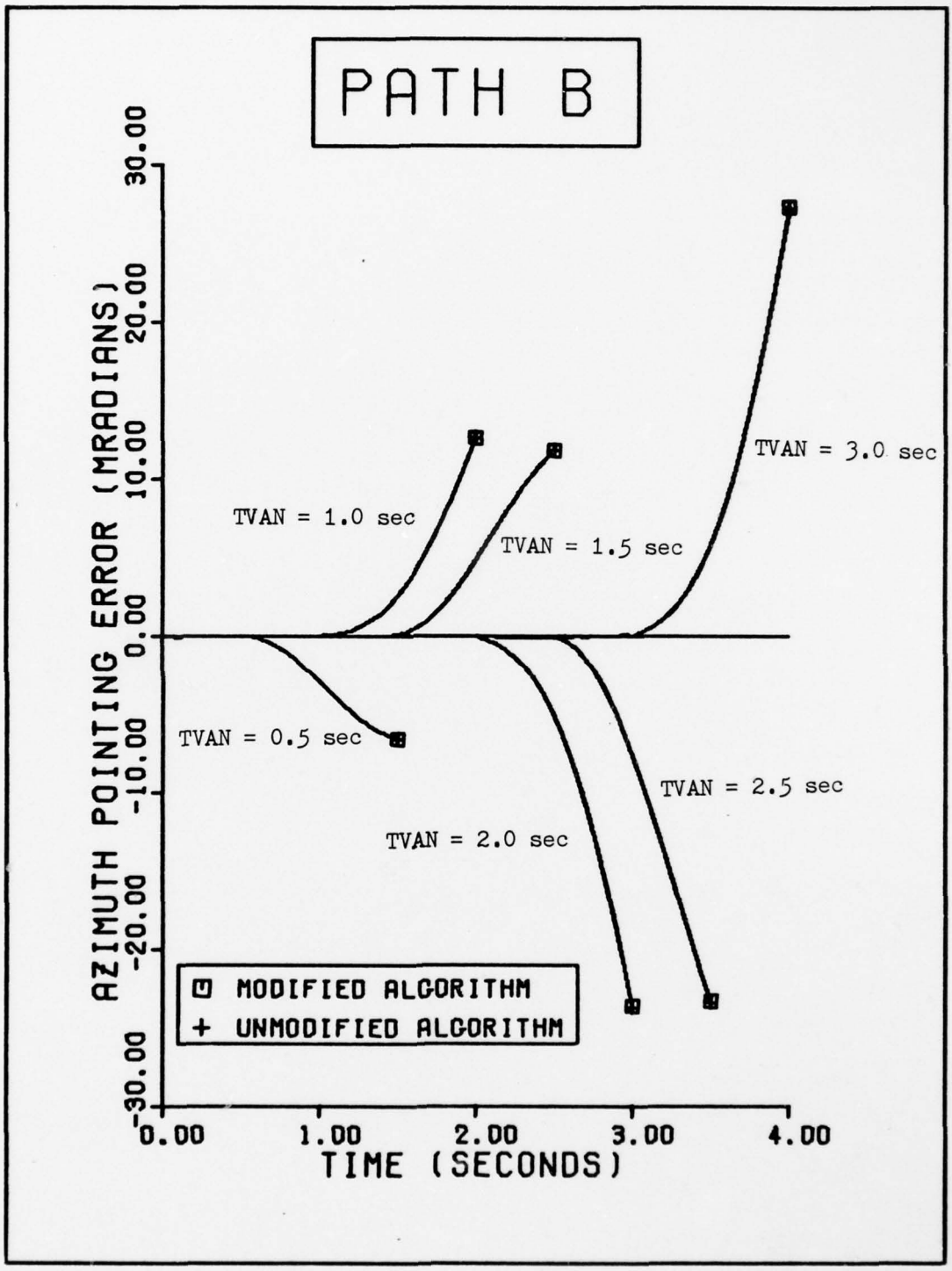


Figure 9. Azimuth Pointing Error versus Time, Various TVAN Times, Path B

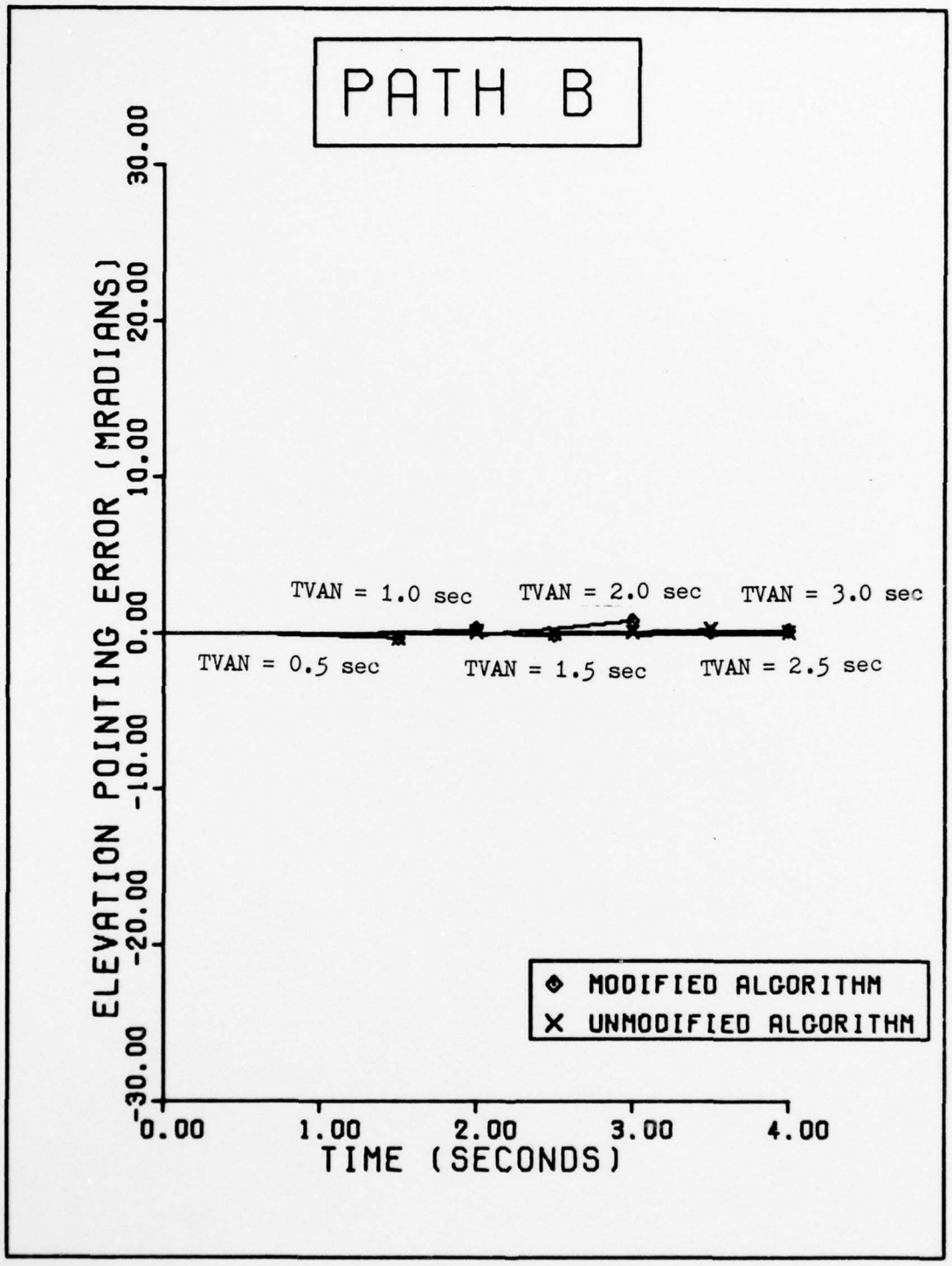


Figure 10. Elevation Pointing Error versus Time, Various TVAN Times, Path B

Table III

Coast Mode RMS Angular Pointing Error Comparison, Path C

TVAN (Seconds)	Channel	Unmodified Algorithm RMS Error (Milliradians)	Modified Algorithm RMS Error (Milliradians)
0.5	Azimuth	3.1699	3.1700
	Elevation	3.1997	3.2002
1.0	Azimuth	3.7443	3.7392
	Elevation	3.5835	3.4873
1.5	Azimuth	1.8031	1.7459
	Elevation	1.8103	1.6521
2.0*	Azimuth	5.8712	5.8629
	Elevation	5.3699	5.2887
2.5	Azimuth	10.3085	10.4500
	Elevation	9.1538	9.1089
3.0	Azimuth	9.4819	9.0621
	Elevation	7.8576	7.6997

*Deceleration Time

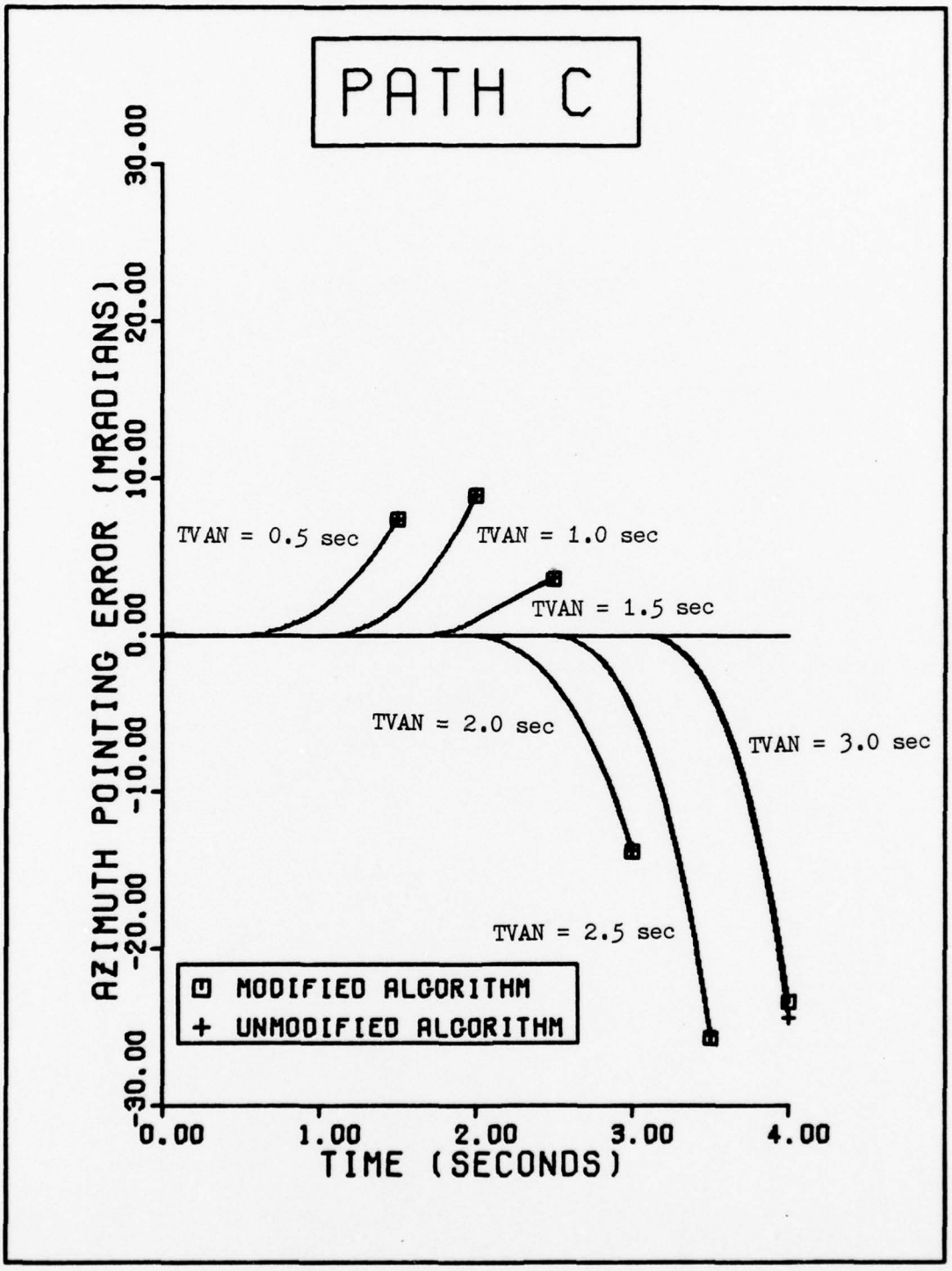


Figure 11. Azimuth Pointing Error versus Time, Various TVAN Times, Path C

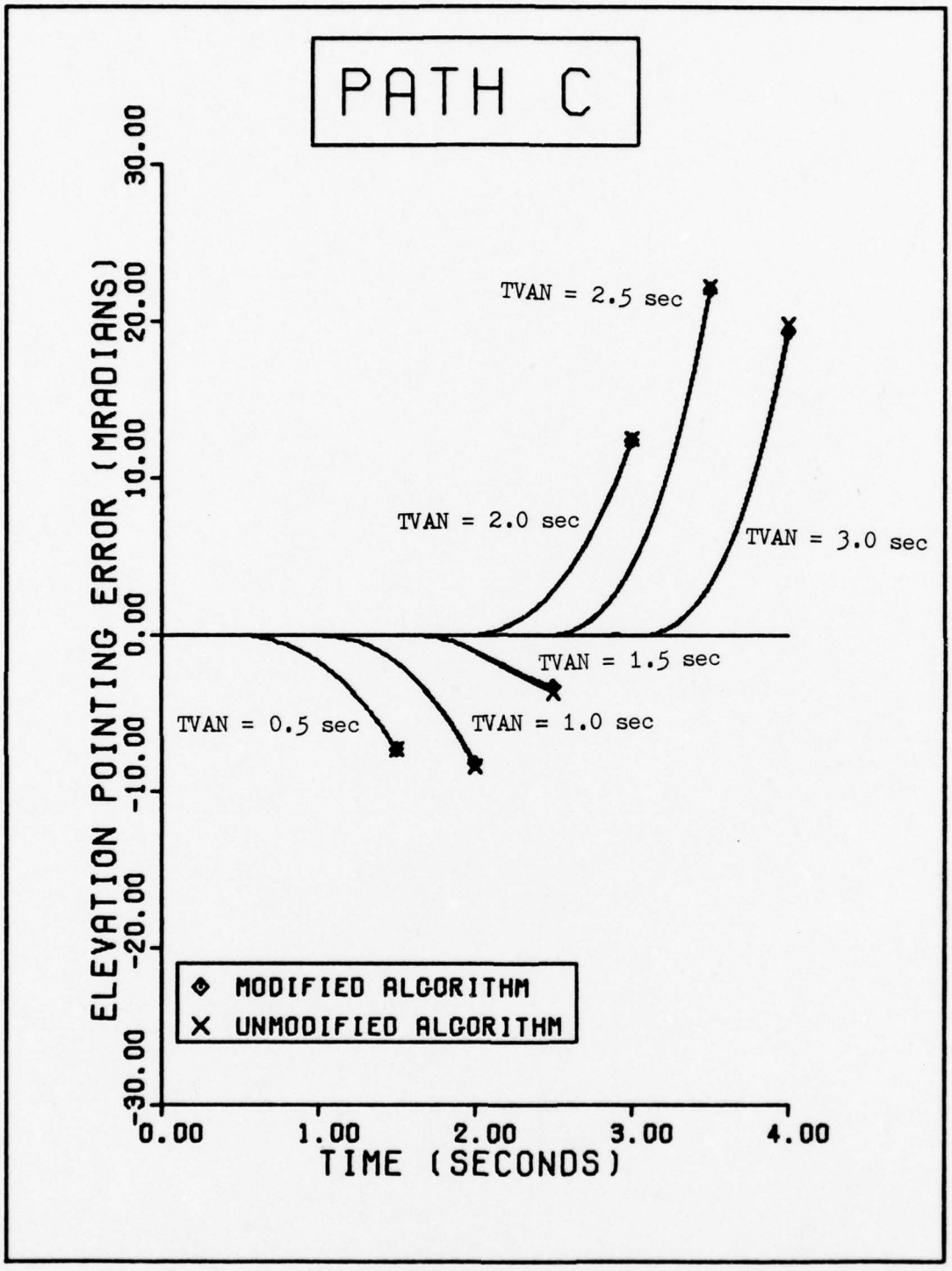


Figure 12. Elevation Pointing Error versus Time, Various TVAN Times, Path C

Discussion

This thesis investigated improving the performance of an aided pointing and tracking system during periods of sensor blackout. It is significant, however, than during the normal modes of operation, prior to t = TVAN in all the computer simulations performed, the pointing error performance of the modified system was virtually identical to that of the original system. This result was obtained because during the short propagation time period of 0.1 seconds, the two different aiding algorithms produced only slightly different target state estimates. These slightly different estimates produced only slightly different aiding signals which, when added to the tracker controller signals, produced almost identical angular rate commands. These commands subsequently resulted in the nearly identical pointing errors.

The difference in performance between the two systems depended on the amount that the estimated acceleration vector was rotated in the modified algorithm. That amount of rotation, $\theta(\Delta T)$, was small because ΔT was only 0.1 seconds.

If extremely large magnitudes of $W_{IU_N}(t)$ occured during the period ΔT, large differences between the performances of the two algorithms would occur. However, $W_{IU_N}(t)$ is limited in magnitude by the aerodynamic and structural limits of the airborne target vehicles. Such limited values of $W_{IU_N}(t)$, integrated over a ΔT of 0.1 seconds, are expected to continue to produce small values of $\theta(\Delta T)$.

Significant differences did occur between the two systems during the coast modes of operation, after t = TVAN. The following subsections discuss these differences at they occured during each target path simulation.

Path A Discussion. The modified system generally performed much better than the original when Path A was simulated. This result was to be expected, because the target motion that was simulated by Path A was exactly the type

of motion that was modeled in the propagation section of the modified algorithm. The modification did not produce exact target tracking during the coast mode periods, however, because the uncertainties in the measurements prevented the zero error target state estimates from being calculated.

Table I illustrates that the degree of improvement shown by the modified system is sensitive to the filter operating time. After 1.3 seconds or more of filter operating time (TVAN = 1.5 seconds or higher), the modification consistantly produced smaller RMS pointing errors in both channels. After 2.8 seconds of filter operating time (TVAN = 3.0 seconds) the modification produced RMS pointing errors that were approximately one third the size of those produced by the original algorithm.

Prior to TVAN = 1.5 seconds, the modified system produced RMS pointing errors that were the same to slightly larger than those that the original system produced. At the earlier times, neither aiding algorithm has had enough operating time to calculate accurate target state estimates. The modified algorithm propagation of these inaccurate estimates created from equivalent to slightly larger errors than the original algorithm propagation of those same inaccurate estimates. The largest amount by which the original system performed better than the modified system occured at TVAN = 1.0 seconds, when the unmodified elevation channel showed an RMS error appoximately 0.0423 milliradians smaller than the modified elevation channel. At all other times prior to TVAN = 1.5 seconds, the performance of the two systems were equivalent.

The reason for these results is graphically illustrated in Fig 13. This figure contains two graphs that plot the actual and estimated values for the X_2 inertial acceleration versus time for each algorithm as Path A is tracked. TVAN = 3.0 seconds for these plots and measurement uncertainties are included. Prior to t = TVAN during the normal mode, the estimated

values for $\ddot{X}_2(t)$ computed by each algorithm are virtually identical. At t = TVAN = 3.0 seconds, however, when the coast mode is initiated, the difference between the two algorithms becomes apparent.

Because the unmodified algorithm models a constant inertial acceleration, the estimated value of $\ddot{X}_2(t)$ remains constant after t = TVAN. The modified algorithm, on the other hand, models a rotating inertial acceleration vector, so after t = TVAN the estimated value of $\ddot{X}_2(t)$ (one component of that rotating acceleration vector) propagates as a changing acceleration. In the case of Path A, this changing estimated acceleration more closely resembles the actual acceleration and the RMS errors are smaller as a result. The characteristics of the acceleration estimates illustrated in Fig 13 are typical of the X_1 and X_2 acceleration estimates computed during all the simulations of Path A.

Fig 14 contains two graphs that plot the actual and estimated values for the X_2 inertial acceleration versus time for each algorithm as Path A is tracked. TVAN = 3.0 seconds, but unlike Fig 13, no measurement uncertainties are included. Comparison of Fig 14 to Fig 13 illustrates that the difference in performance found between the original and modified algorithms is caused by the different propagation methods utilized by each. The same result is obtained from the perfect measurement case as from the uncertain measurement case except that the acceleration estimates are slightly less accurate in the uncertainty case. Because the results of these two cases are similar and because any other set of uncertainty sequences with the same zero means and standard deviations is expected to be very similar to this set, it can be concluded that only one set of uncertainties need be investigated in this study to produce a general result. Fig 14 is typical of the perfect measurement simulations performed in this study.

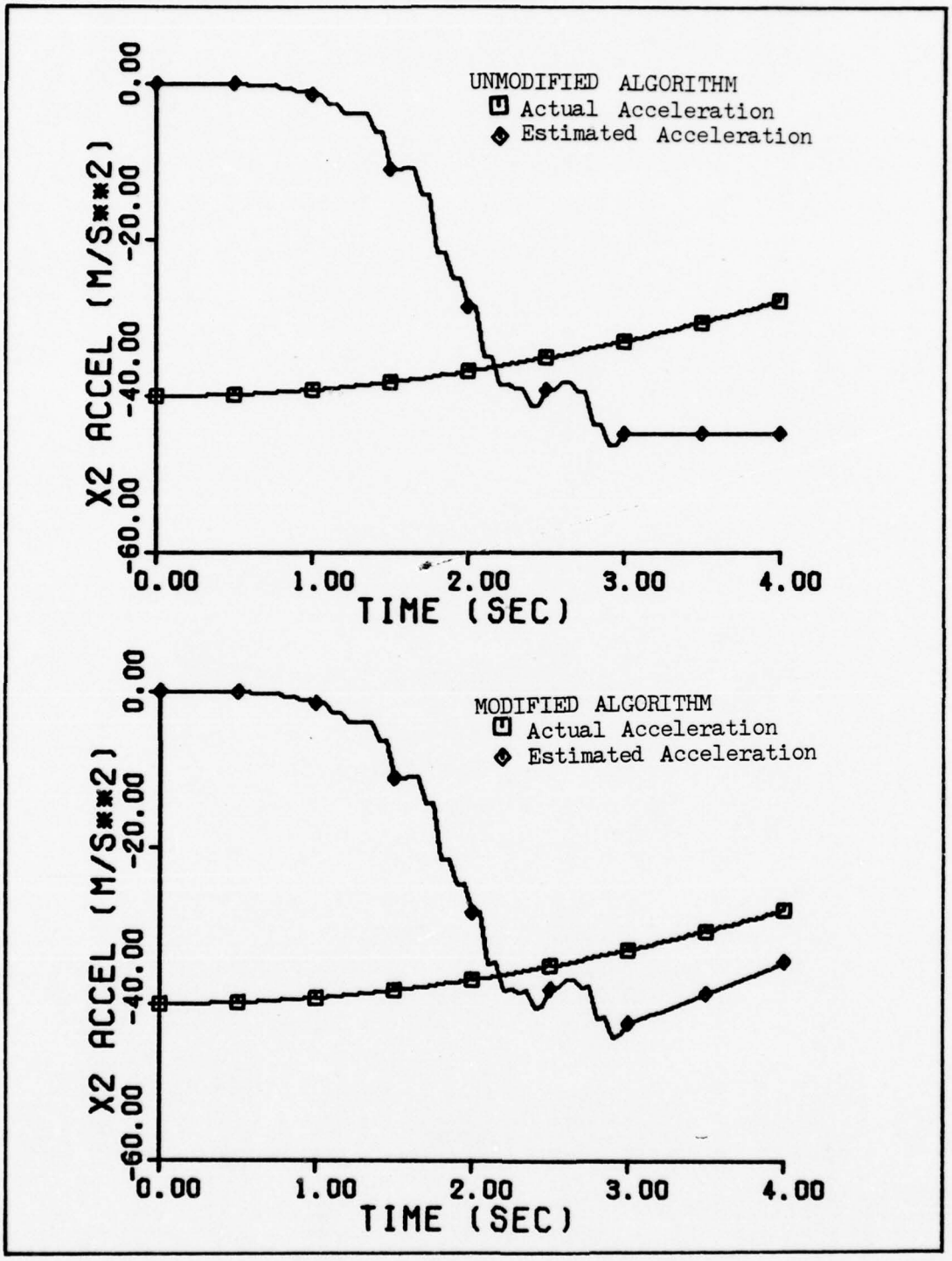


Figure 13. Actual and Estimated Magnitudes of $\ddot{X}_2(t)$, Path A, TVAN = 3.0 Seconds, for Unmodified and Modified Algorithms, Measurement Uncertainties Included

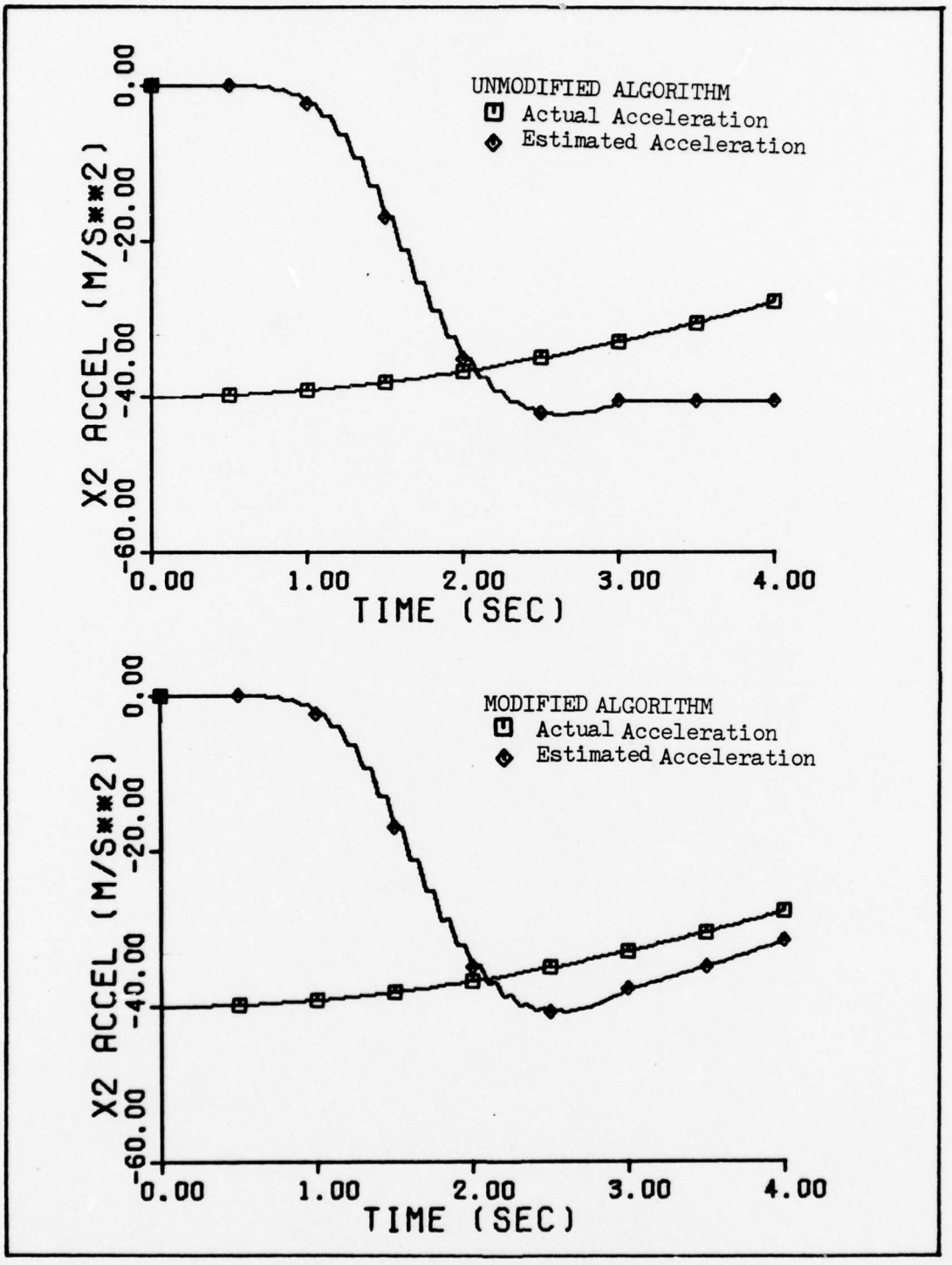


Figure 14. Actual and Estimated Magnitudes of $\ddot{X}_2(t)$, Path A, TVAN = 3.0 Seconds, for Unmodified and Modified Algorithms, Measurement Uncertainties Not Included

Path B Discussion. The performance of the modified and unmodified systems during the simulation of Path B were equivalent. Observation of the azimuth errors listed in Table II shows that neither method was clearly superior. At different times each showed slightly better performance than the other, but no trends indicating one aiding algorithm better overall are found in the results.

The rapidly changing target states of Path B could not accurately be calculated by the Kalman filter because the filter bandwidth was too narrow to respond satisfactorilly to the 0.5 Hertz target oscillations. Consequently, the state estimates used to compute the aiding signals were grossly inaccurate in both algorithms.

When a coast mode period would begin at t = TVAN, the two algorithms propagated those erroneous estimates into the future by two different methods. The state estimates obtained from each algorithm after this process were different from each other, but they were both even more different from the true target states. Also, the target motion encountered during the simulation of Path B was not modeled properly in either algorithm because the acceleration was not constant in either inertial or body fixed coordinates. Because each algorithm started the coast mode with equally poor estimates of the true target states, because neither algorithm properly modeled the target dynamics, and because the two estimated target states produced by the different algorithms were much more closely equal to each other than to the true target state, the resulting RMS azimuth errors produced by both systems were nearly equal.

The RMS azimuth errors increased as TVAN increased. This occured because as the target moved closer to the tracker, the required tracker angular deflections and rates needed to properly track the oscillating target increased.

The RMS elevation errors listed in Table II illustrate the measurement uncertainty effects on the operation of the two aiding algorithms. No target motion took place out of the X_1X_2 inertial plane, therefore all the elevation errors listed were caused strictly by the measurement uncertainties, not target dynamics or system dynamic lag. Those uncertainties created erroneous target motion estimates that propagated out of the X_1X_2 plane, causing elevation rate commands which, in turn, caused elevation channel errors. In the elevation channel, neither algorithm showed more sensitivity to the measurement uncertainties; each algorithm showed better elevation channel performance at different TVAN times.

Path C Discussion. The performance of the two systems during the simulation of Path C were equivalent. Table III illustrates that at various TVAN times, each system produced RMS pointing errors that were slightly smaller than those produced by the other. However, neither system showed an overall superior performance.

This equivalent performance is not surprising, because the target model that was incorporated into the original algorithm perfectly modeled the actual target motion (disregarding the instantaneous acceleration change at t = 2.0 seconds). Also, the modified algorithm was designed to switch to the original propagation method in cases, such as Path C, when $A_L(t) = 0$.

If the algorithms had produced perfect state estimates, the modified algorithm would have calculated $A_L(t) = 0$, and the original method portion of the modified algorithm would have been switched on. However, because of the measurement uncertainties, an estimated value of $A_L(t) \neq 0$ was calculated and the modified algorithm propagated the current state estimates differently than the original algorithm.

These calculated estimated values of $A_L(t)$ were small, though, so that the estimates resulting from the modified algorithm propagation were close

to those resulting from the original propagation. Thus, the aiding signals and subsequent RMS pointing errors were close to the same values.

The smallest RMS pointing errors produced by both systems occured during the coast mode period that started at TVAN = 1.5 seconds. This result illustrates that both algorithms were producing increasingly better estimates of the $-X_1$ acceleration as the operating times of the filters increased. If the acceleration of the target had remained constant, it is expected that both algorithms would continue to produce increasingly better, nearly equivalent, state estimates, and the values of subsequent one second coast mode period RMS errors would show even better performance.

VI. Conclusions and Recommendations

This chapter lists the conclusions formulated during this investigation and recommends areas for further study.

Conclusions

1. The coast mode performance of the particular aided pointing and tracking system studied in this thesis can be improved, under certain conditions, by making a simple software modification to the aided track algorithm. This modification incorporates a body fixed, rotating coordinate system into the propagation portion of the aided track algorithm. The coast mode performance of this particular modification does not show improvement under all conditions, but the resulting performance is always at least equivalent to the original system performance.

2. The software modification suggested by this thesis can be incorporated into the system without degrading normal mode performance of the system.

3. The suggested modification has the same sensitivity to measurement uncertainties as the original system.

Recommendations

1. A follow-on study to this investigation should be performed that utilizes a more sophisticated propagation model. This new model should not be constrained merely to rotate a constant magnitude, inertial acceleration vector about a body fixed axis as the model in this investigation. Rather the new model should allow the effects of a changing body fixed acceleration (changed by target roll or changes in thrust or angle of attack) to be propagated.

2. A follow-on study to this investigation should be performed that checks the validity of the assumption made in this thesis that the effects of gravity can be detected and compensated for. This suggested study should proceed by investigating the errors that would create uncertainties in the estimates of the true magnitude and direction of the acceleration due to gravity. The performance of the pointing and tracking system as it processes these erroneous gravity estimates could then be investigated.

3. This investigation assumed one set of measurement error values. The relative sensitivity of the aided pointing and tracking system to different sets of measurement errors was not studied. A study should be performed that investigates changes in performance caused by changing the quality (and thus the accuracy) of the sensing devices used on the system.

4. This thesis did not investigate the effects on the performance of the pointing and tracking system that adding or removing different sensing devices would cause. A follow-on study should be performed that studies different measurement devices and their effects on the system.

5. A follow-on study to this investigation should be performed that investigates the effects of individual sensor blackouts on the system pointing error performance. This thesis studied only the effects of

complete, simultaneous sensor losses. In actual practice, however, sensors may fail individually so that some valid sensor measurements would still be available. The performance of the pointing and tracking system under those conditions should be studied.

Bibliography

1. Fitts, John M. A Strapdown Approach to HAT Aided Tracking, Culver City, California: Aerospace Group, Hughes Aircraft Company, September 1971.

2. School of Mechanical and Aerospace Engineering, Oklahoma State University. Studies of Advanced Simulation Concepts, User Manual for OSUAPT-3.1 and FRQAPT, Volume I. Report Number ER-75-R-109-004, produced under United States Air Force Contract F29601-75-C-0121. Stillwater, Oklahoma: Oklahoma State University, March 1976.

3. Sebesta, H. R. and L. R. Ebbesen. Studies of Advanced Simulation Concepts, Technical Results and Modeling Details, Volume I. United States Air Force Report AFWL-TR-74-32, Volume I. Stillwater, Oklahoma: Oklahoma State University, October 1974.

4. Wrigley, Walter, W. M. Hollister and W. G. Denhard Gyroscopic Theory, Design, and Instrumentation, Cambridge, Massachusetts: The M. I. T. Press, 1969.

Appendix A

Computer Program Modification Listings

The modifications to the original computer program were incorporated into the program by utilizing the CDC UPDATE utility program available on the CDC 6600 computer located at Wright-Patterson Air Force Base, Ohio. The following listings were divided into functional groupings and are presented here to illustrate exactly how the original program (described in Ref 2) was modified.

Basic Algorithm Modification

The results of Chapter III of this thesis were coded and inserted into the original program as illustrated below.

```
*INSERT AIDTRK.20
      DIMENSION VOXAO(3),UN(3),UL(3),UV(3)
*INSERT AIDTRK.208
CCC        COMPUTE ANGLE BETWEEN PRESENT EST VEL AND ACCEL VECTORS
      DOTAV=C(2,1)*C(3,1)+C(2,2)*C(3,2)+C(2,3)*C(3,3)
      AMAGO=SQRT(C(3,1)**2+C(3,2)**2+C(3,3)**2)
      IF(ABS(AMAGO).LT.1.0E-3)GO TO 599
      VMAGO=SQRT(C(2,1)**2+C(2,2)**2+C(2,3)**2)
      IF(ABS(VMAGO).LT.1.0E-3)GO TO 599
      CALPHA=DOTAV/(AMAGO*VMAGO)
      ALPHA=ACOS(CALPHA)
      SALPHA=SIN(ALPHA)
      IF(ABS(SALPHA).LT.1.0E-3)GO TO 599
CCC        COMPUTE UNIT VECTOR U-SUB-V (UV) IN INERTIAL COORDS
      DO 560 I=1,3
560   UV(I)=C(2,I)/VMAGO
CCC        COMPUTE UNIT VECTOR U-SUB-N (UN) IN INERTIAL COORDS
      VOXAO(1)=C(2,2)*C(3,3)-C(2,3)*C(3,2)
      VOXAO(2)=C(2,3)*C(3,1)-C(2,1)*C(3,3)
      VOXAO(3)=C(2,1)*C(3,2)-C(2,2)*C(3,1)
      VOXAOM=SQRT(VOXAO(1)**2+VOXAO(2)**2+VOXAO(3)**2)
      DO 570 I=1,3
570   UN(I)=VOXAO(I)/VOXAOM
CCC        COMPUTE UNIT VECTOR U-SUB-L (UL) IN INERTIAL COORDS
      UL(1)=UN(2)*UV(3)-UN(3)*UV(2)
      UL(2)=UN(3)*UV(1)-UN(1)*UV(3)
      UL(3)=UN(1)*UV(2)-UN(2)*UV(1)
```

```
CCC       COMPUTE COMPONENTS OF ACCEL IN U COORD SYSTEM
      AVM=AMAGO*CALPHA
      ALM=AMAGO*SALPHA
CCC       COMPUTE THETA
      IF(ABS(AVM).LT.1.0E-6)GO TO 580
      ARGMT=AVM*DTT/VMAGO+1
C         (CHECK FOR NEGATIVE OR ZERO ARGUMENT OF NATURAL LOG)
      IF(ARGMT.LE.0)GO TO 580
      THETA=ALM*ALOG(ARGMT)/AVM
      GO TO 590
580   THETA=ALM*DTT/VMAGO
590   CTH=COS(THETA)
      STH=SIN(THETA)
CCC       COMPUTE NEW ACCEL ESTIMATE
      DO 600 I=1,3
600   EX(3,I)=(AVM*CTH-ALM*STH)*UV(I)+(AVM*STH+ALM*CTH)*UL(I)
CCC       COMPUTE NEW VEL ESTIMATE
      VMAGN=AVM*DTT+VMAGO
      DO 610 I=1,3
610   EX(2,I)=VMAGN*CTH*UV(I)+VMAGN*STH*UL(I)
CCC       COMPUTE NEW POS ESTIMATE
      RI=    (VMAGO/2+(AVM*DTT+VMAGO)*CTH/2)*DTT
      RJ=    ((AVM*DTT+VMAGO)*STH/2)*DTT
      DO 650 I=1,3
650   EX(1,I)=RI*UV(I)+RJ*UL(I) +C(1,I)
      DO 660 I=1,3
      DO 660 J=1,3
      IVINC=3.*(J-1.)+(I-1.)+250
      X(IVINC)=EX(I,J)
      JVINC=IVINC+13
660   X(JVINC)=G(I,J)
      GO TO 210
599   CONTINUE
```

Path Simulation

The following statements simulated each target path by specifying the time history of the inertial acceleration to be applied to the target. The computer simulation integrated these accelerations to compute the target velocity and position for later use in the simulation. Following each set of program statements is presented the initial condition matrix for that particular path. The computer variable names given to the $X_1X_2X_3$ set of inertial target states is given by

$$\bar{X}(t) = \begin{bmatrix} X_1(t) & X_2(t) & X_3(t) \\ \dot{X}_1(t) & \dot{X}_2(t) & \dot{X}_3(t) \\ \ddot{X}_1(t) & \ddot{X}_2(t) & \ddot{X}_3(t) \end{bmatrix} = \begin{bmatrix} X(09) & X(12) & X(15) \\ X(10) & X(13) & X(16) \\ X(11) & X(14) & X(17) \end{bmatrix} \quad (34)$$

Units of position, velocity, and acceleration are meters, meters/second, and meters/second^2, respectively. A complete description of the target paths is given in Appendix B.

Path A.

```
*INSERT TARBAS.9
      X(14)=-40*COS(TIME/5)
      X(17)=-40*SIN(TIME/5)
```

$$\bar{X}(0) = \begin{bmatrix} 1000.0 & 1000.0 & 0.0 \\ 200.0 & 0.0 & 0.0 \\ 0.0 & 0.0 & 0.0 \end{bmatrix} \quad (35)$$

Path B.

```
*INSERT TARBAS.9
      PIT=3.14159265 *TIME
      X(11)=-2.654451328*SIN(2*PIT)
      X(14)=-100*SIN(PIT)
```

$$\bar{X}(0) = \begin{bmatrix} 4000.0 & 0.0 & 0.0 \\ -599.577531 & 31.83098861 & 0.0 \\ 0.0 & 0.0 & 0.0 \end{bmatrix} \tag{36}$$

Path C.

```
*INSERT TARBAS.9
      IF(TIME.LT.2.) X(11)=-300
      IF(TIME.GE.2.) X(11)=40
```

$$\bar{X}(0) = \begin{bmatrix} 5000.0 & 1000.0 & 1000.0 \\ -250.0 & 0.0 & 0.0 \\ -300.0 & 0.0 & 0.0 \end{bmatrix} \tag{37}$$

Coast Mode Simulation

The coast mode was simulated by defining a variable flag, ICOAST, which was set to FALSE when the normal mode was to be simulated and set to TRUE when the coast mode was to be simulated. The original program defined two additional variable flags, MIROT and IROT, which were utilized to check if the simulated target was detected in the tracker field of view or the tracker gate, respectively. (Ref 2:28-31)

Through the use of multiple IF statements, when the coast mode was selected (ICOAST = FALSE), then MIROT and IROT were set to FALSE, even if the target was actually located in the field of view or gate, to simulate sensor failure. When these two flags became FALSE, the tracker was forced into a search mode, increasing the size of the field of view in order to look for the target.

The rate memory function of the coast mode was simulated by setting all the pointing error samples to zero so that the proportional plus integral tracker controller command was held constant at a value equal to the last integrator output. Also during the coast mode period, the Kalman filter update equations were by-passed by an IF and GO TO statement to avoid calculations with erroneous data. The following computer statements were used to simulate the coast mode.

```
*INSERT TI.7
      COMMON/COAST/ICOAST
*INSERT TI.37
      ICOAST=FALSE
CCC       INSERT TVAN AND TREAP HERE CCC
      TVAN=1.0
      TREAP=5.1
*DELETE TI.82
10    IF(TIME.LT.TVAN.OR.TIME.GE.TREAP)GO TO 11
      ICOAST=TRUE
      IROT=FALSE
      MIROT=FALSE
      GO TO 12
11    ICOAST=FALSE
12    IF(TIM10.EQ.0)GO TO 150
```

```
*DELETE TI.87
30    IF(IROT.EQ.TRUE.AND.ICOAST.EQ.FALSE)GO TO 35
*DELETE TI.91
*DELETE TI.92
*DELETE TI.100
      IF(MIROT.EQ.TRUE.AND.ICOAST.EQ.FALSE)GO TO 100
*DELETE TI.102
60    IF(ICOAST.EQ.FALSE)MIROT=TRUE
*DELETE TI.178
      IF(ICOAST.EQ.FALSE)MIROT=TRUE
*DELETE TI.183
      IF(ICOAST.EQ.FALSE)IROT=TRUE
*DELETE TI.214
      IF(ICOAST.EQ.FALSE)IROT=TRUE
*DELETE TI.234
      IF(ICOAST.EQ.FALSE)MIROT=MIN0(ISMPLL,ISAMP_)
*DELETE TI.242
240   IF(ICOAST.EQ.FALSE) GO TO 241
      ERAZS=0
      ERELS=0
      ERAZL=0
      ERELL=0
241   WCAZ=A9*(X(76)+A8*ERAZS)
*INSERT AIDTRK.7
      COMMON/COAST/ICOAST
*DELETE AIDTRK.285
310    IF(ICOAST.EQ.-1)GO TO 130
      CALL KALMAN
```

Uncertainties

The range, pointing error, and gyro bias drift uncertainties were simulated as follows. (GAUSS is the subroutine that calculated the three sets of normal, zero mean measurement errors that were added to the range and pointing error measurements.)

Range.

```
*INSERT AIDTRK.14
      COMMON /RANGE/ RR(3)
*DELETE AIDTRK.82
      RR(3)=RR(2)
      RR(2)=RR(1)
      CALL GAUSS(1,1,0.,5.)
      RR(1)=R+X(231)
*DELETE AIDTRK.123
      ERD=(3*RR(1)-4*RR(2)+RR(3))/(2*DT)
*DELETE AIDTRK.286
      CALL GAUSS(1,1,0.,5.)
      RR(1)=R+X(231)
*INSERT APTXVA.12
      COMMON /RANGE/ RR(3)
      DIMENSION RR(3)
*INSERT APTXVA.196
      IF(ATENA.NE.0.OR.TIM10.EQ.0) GO TO 500
      RR(3)=RR(2)
      RR(2)=RR(1)
      CALL GAUSS(1,1,0.,5.)
      RR(1)=R+X(231)
500   CONTINUE
```

(Where the units of range measurement are meters.)

Pointing Error.

```
*DELETE TI.170
160   CALL GAUSS(2,1,0.,.00001)
      AZER=1000.0*(ERAZ+X(232))
*DELETE TI.175
      CALL GAUSS(3,1,0.,.00001)
      ELER=1000.0*(ERFL+X(233))+TESOS
```

(Where the units of angle measurement are radians.)

Gyro Bias Drift.

```
*DELETE APTDYA.71
      DY(1)=WCAZL-WID-AZGC+4.8481368E-7
*DELETE APTDYE.70
      DY(31)=WCELL-WIE-ELGC+4.8481368E-7
```

(Where 0.1 degrees/hour = 4.8481368×10^{-7} radians/second.)

Additional Output

The following statements were inserted in order to provide additional output data not provided by the original program. They are listed here for information only.

```
*INSERT TIMRSP.75
605    FORMAT(1X,F5.2,5(E12.4))
606    FORMAT(1X,5(E12.4))
       NUMBER=1
       JCHECK=0
       WRITE(15,605)TIME,X(11),X(14),X(17),AM,E1
       WRITE(15,606)E2,E3,EM,THETAD,X(4),X(8)
*INSERT TIMRSP.151
       IF(TIME.LT.X(81))GO TO 601
       IF(JCHECK.EQ.1)GO TO 601
       SAZ=SIN(X(1))
       CAZ=COS(X(1))
       SEL=SIN(X(5))
       CEL=COS(X(5))
       C11=CAZ*CEL
       C12=-CAZ
       C13=CAZ*SEL
       C21=SAZ*CEL
       C22=CAZ
       C23=SAZ*SEL
       C31=-SEL
       C33=CEL
       JCHECK=1
601    E1=C11*X(252)+C12*X(255)+C13*X(258)
       E2=C21*X(252)+C22*X(255)+C23*X(258)
       E3=C31*X(252)+C33*X(258)
       AM=SQRT(X(11)**2+X(14)**2+X(17)**2)
       EM=SQRT(E1**2+E2**2+E3**2)
       AMDOTEM=X(11)*E1+X(14)*E2+X(17)*E3
       IF(ABS(AM).LT.1.0E-10.OR.ABS(EM).LT.1.0E-10)GO TO 603
       CTHETA=AMDOTEM/(AM*EM)
       THETA=ACOS(CTHETA)
       THETAD=(THETA*180)/3.14159 26536
       GO TO 604
603    THETAD=0.0
604    WRITE(15,605)TIME,X(11),X(14),X(17),AM,E1
       WRITE(15,606)E2,E3,EM,THETAD,X(4),X(8)
       NUMBER=NUMBER+1
*INSERT TIMRSP.215
607    FORMAT(1X,I6)
       WRITE(14,607)NUMBER
```

Program Corrections

The following statements corrected programming errors that were present in the original program available at Wright-Patterson Air Force Base, Ohio. They are listed here for information only.

```
*DELETE TIMINP.152
      IF(NTAB.LE.0)GO TO 385
*INSERT TIMINP.197
385   CONTINUE
*INSERT TIMINP.204
      GO TO 420
*INSERT TIMMDL.8
      NS=X(208)
*INSERT TIMMDL.9
      CALL APTINI
*INSERT TIMMDL.12
      CALL APTDYA
      CALL APTDYE
*INSERT TIMMDL.15
      CALL APTXVA
      CALL STATS
*INSERT TIMMDL.18
      CALL APTLIN(TSTP,0)
*INSERT TIMMDL.21
      CALL APTMON
*DELETE APTBLK.49
      DATA IYD/16,24,25,26,27,28,29,30,132*0/
*DELETE KALMAN.28
*DELETE KALMAN.42
```

Appendix B

Simulated Target Paths

Three representative target paths were devised. By comparing the modified algorithm system performance with that of the unmodified system as each path was tracked, any improvement or degradation due to the modification could be found.

The tracker base was simulated to be stationary during all computer runs. All target paths were defined in relation to an arbitrary inertial coordinate system with the three primary directions of X_1, X_2, and X_3. The origin of the coordinate system was defined to coincide with the tracker.

Path A

The first simulated path was designated Path A, and it represented a circular target path with a 1000 meter radius contained in a plane perpendicular to the X_1 inertial axis at a distance of 1000 meters from the tracker, centered on the X_1 axis. The speed of the target was maintained at 200 meters/second and the target acceleration was maintained at a constant magnitude of 40 meters/second^2. The target acceleration was always directed toward the center of the circle. The acceleration applied to the target in Path A was equal to approximately 4.08 g.

Path B

The second simulated path was designated Path B, and it represented a constant speed, sinusoidal target path completely contained in the X_1X_2 inertial plane. At t = 0, the target was located 4000 meters from the tracker on the X_1 axis. Subsequent motion oscillated at a frequency of

0.5 Hertz about the X_1 axis toward the tracker. The speed of the target was maintained constant at approximately 600.42 meters/second. The acceleration of the target in the X_1 direction varied from approximately -0.27 g to +0.27 g. The acceleration of the target in the X_2 direction varied from approximately +4.08 to -4.08 g.

Path C

The final simulated path was designated Path C. It represented the path of a target that was accelerated for 2.0 seconds along a straight line by an approximate 30.61 g acceleration, then decelerated in the same direction by an approximate -4.08 g acceleration. The target was initially located at a point 5000 meters in the X_1 direction and 1000 meters in the X_2 and X_3 directions from the tracker. The target moved in the negative X_1 direction, parallel to the X_1 axis.

Fig 6 illustrates the three target paths simulated during the investigation of this thesis. Initial conditions for each path are listed in Appendix A under the subsection, Path Simulation.

VITA

James G. Terry was born on 30 November 1945 in Rapid City, South Dakota. His father was a member of the United States Air Force, and, consequently, he lived and attended school in several different states plus Germany and Japan until he graduated from high school in Phoenix, Arizona, in 1963. He attended Arizona State University for one year then transferred to the United States Air Force Academy (USAFA). In June 1968 he graduated from USAFA with a Bachelor of Science in Engineering Sciences and was commissioned in the United States Air Force. He completed pilot training and received his wings in August 1969, then served as a Strike F-105D pilot at McConnell Air Force Base, Kansas, until December of 1971. In 1972 he trained to become a Wild Weasel F-105G pilot and then served for a year in Thailand. During that year he flew 122 combat missions in the F-105G, 87 of them over North Vietnam. He returned from overseas to George Air Force Base, California, in February 1973 where he continued to fly F-105G aircraft until he entered the School of Engineering, Air Force Institute of Technology, in June 1976. He is a member of Tau Beta Pi, the National Engineering Honor Society.

Permanent address: 6420 West Roma Avenue
Phoenix, Arizona
85033

Unclassified

SECURITY CLASSIFICATION OF THIS PAGE *(When Data Entered)*

REPORT DOCUMENTATION PAGE		READ INSTRUCTIONS BEFORE COMPLETING FORM
1. REPORT NUMBER AFIT/GA/EE/77-6	2. GOVT ACCESSION NO.	3. RECIPIENT'S CATALOG NUMBER
4. TITLE *(and Subtitle)* IMPROVING AIDED TRACK PERFORMANCE DURING PERIODS OF TRACKER SENSOR FAILURE BY UTILIZING A TARGET BODY FIXED COORDINATE SYSTEM		5. TYPE OF REPORT & PERIOD COVERED MS Thesis 6. PERFORMING ORG. REPORT NUMBER
7. AUTHOR*(s)* James G. Terry Captain USAF		8. CONTRACT OR GRANT NUMBER*(s)*
9. PERFORMING ORGANIZATION NAME AND ADDRESS Air Force Institute of Technology (AFIT-EN) Wright-Patterson AFB, Ohio 45433		10. PROGRAM ELEMENT, PROJECT, TASK AREA & WORK UNIT NUMBERS
11. CONTROLLING OFFICE NAME AND ADDRESS Air Force Weapons Laboratory (AFWL/LRO) Kirtland AFB, NM 87117		12. REPORT DATE December, 1977 13. NUMBER OF PAGES 68
14. MONITORING AGENCY NAME & ADDRESS*(if different from Controlling Office)*		15. SECURITY CLASS. *(of this report)* Unclassified 15a. DECLASSIFICATION/DOWNGRADING SCHEDULE

16. DISTRIBUTION STATEMENT *(of this Report)*

Approved for public release; distribution unlimited

17. DISTRIBUTION STATEMENT *(of the abstract entered in Block 20, if different from Report)*

18. SUPPLEMENTARY NOTES

Approved for public release; IAW AFR 190-17

JERRAL F. GUESS, Captain, USAF
Director of Information

19. KEY WORDS *(Continue on reverse side if necessary and identify by block number)*

Kalman Filter
High Accuracy Tracking
Aided Track
Body Fixed Axes
Sensor Failure
Coast Mode Tracking

20. ABSTRACT *(Continue on reverse side if necessary and identify by block number)*

A new target acceleration model capable of improving the performance of an airborne aided track system during periods of tracker sensor failure was investigated. An aided track target prediction algorithm utilizing range and angle rate measurements was modified so that the target state estimates were propagated by integrating the estimated constant, body fixed acceleration.

The modified algorithm performance was compared to the original by simulating three target paths. At specified times, all tracking sensors were turned off to simulate sensor failure. Each algorithm attempted to

DD FORM 1 JAN 73 1473 EDITION OF 1 NOV 65 IS OBSOLETE

Unclassified

SECURITY CLASSIFICATION OF THIS PAGE *(When Data Entered)*

Block 20 (continued)

keep the target centered on the tracker boresight by extrapolating target position estimates without processing any measurements. RMS pointing errors were computed for the one second periods following each failure.

During normal sensor operations, the performance of the modified algorithm was equivalent to the original. When the sensors were failed during the tracking of targets following a constant, body fixed acceleration, the modified algorithm generally produced smaller RMS errors. (After 2.8 seconds of filter operating time, the modified algorithm produced one third the RMS error of the original.) When sensor failure occured during the tracking of targets following a rapidly oscillating path or traveling in a straight line under large linear accelerations, both algorithms produced equivalent RMS errors. The modified algorithm demonstrated the same sensitivity to measurement uncertainties as the original.